

1 **Title**

2 PD-1 aborts the activation trajectory of autoreactive CD8<sup>+</sup> T cells to prohibit their acquisition of effector  
3 functions

4

5 **Authors**

6 Hikari Okamura<sup>a,b</sup>, Il-mi Okazaki<sup>a</sup>, Kenji Shimizu<sup>a</sup>, Takumi Maruhashi<sup>a</sup>, Daisuke Sugiura<sup>a</sup>, Reina  
7 Mizuno<sup>a</sup>, Taku Okazaki<sup>a,\*</sup>

8

9 **Affiliations**

10 <sup>a</sup>Division of Immune Regulation, Institute of Advanced Medical Sciences, Tokushima University,  
11 Tokushima 770-8503, Japan

12 <sup>b</sup>Immunology Research Unit, Department of Medical Innovations, Otsuka Pharmaceutical Co., Ltd.,  
13 Tokushima 771-0130, Japan

14

15 \*Corresponding author. Division of Immune Regulation, Institute of Advanced Medical Sciences,  
16 Tokushima University, 3-18-15 Kuramoto, Tokushima, 770-8503, Japan. E-mail address:  
17 tokazaki@genome.tokushima-u.ac.jp (T. Okazaki).

18

1 **Abstract**

2 Anti-PD-1 therapy can induce eradication of tumors and immune-related adverse events (irAEs) in  
3 humans and model animals. However, how anti-PD-1 therapy modifies cellular phenotypes of CD8<sup>+</sup> T  
4 cells to destroy tumors and damage self-tissues remains to be clarified. Here we performed single-cell  
5 mRNA expression profiling of autoreactive CD8<sup>+</sup> T cells under or beyond PD-1 suppression in target  
6 tissues and reconstructed their activation trajectory. Autoreactive CD8<sup>+</sup> T cells went through four  
7 activation phases and PD-1 strongly attenuated the transition from the second- to the third-phase, where  
8 effector functions were acquired. Shifts in cluster composition of autoreactive CD8<sup>+</sup> T cells markedly  
9 reflected the severity of autoimmunity. In addition, genes up-regulated along the activation-trajectory in  
10 autoimmunity were highly expressed in responders of melanoma patients in anti-PD-1 therapy,  
11 suggesting that tumor-specific T cells need to be activated in a similar trajectory to destroy tumors in  
12 human patients upon PD-1 blockade. These findings reveal that PD-1 blockade facilitates the activation  
13 trajectory of CD8<sup>+</sup> T cells to boost their effector functions. Targeted manipulation of the trajectory could  
14 lead to new therapeutic opportunities.

15

16 **Keywords:**

17 PD-1; Type I diabetes; single cell analysis; pseudotime ordering

18

## 1 **1. Introduction**

2 Due to the success of anti-PD-1 therapy in the treatment of cancer with the occasional development of  
3 immune-related adverse-events (irAEs), PD-1 is widely accepted as an immune-checkpoint receptor  
4 that serves to restrict immune responses against self-tissues and tumor cells [1-6]. However, it remains  
5 unclear how PD-1 modifies cellular phenotypes of T cell specific to self- and tumor-antigens to avoid  
6 autoimmunity and hamper tumor eradication.

7 Engagement of PD-1 with either PD-L1 or PD-L2 during antigen stimulation results in the  
8 phosphorylation of two tyrosine residues in the cytoplasmic region of PD-1, the recruitment of protein  
9 tyrosine phosphatase, SHP-2 to the distal phospho-tyrosine, and the decreased phosphorylation of  
10 various signaling molecules. Thereby, PD-1 inhibits T cell receptor (TCR)-dependent activation of T  
11 cells to suppress their proliferation, cytokine production, and cytotoxicity [7-11]. Besides, PD-1 has  
12 been reported to induce anergy and exhaustion of T cells or instruct the differentiation of regulatory T  
13 cells [12-15]. Therefore, anti-PD-1 therapy is presumed to activate T cells by abrogating these PD-1  
14 functions in the eradication of tumors as well as destruction of self-tissues.

15 Actually, PD-1 blockade has been shown to increase the number of antigen specific CD8<sup>+</sup> T  
16 cells in mouse models of chronic viral infection [14-17]. These CD8<sup>+</sup> T cells showed higher capacity to  
17 produce cytokines such as IFN $\gamma$  and TNF upon *ex vivo* re-stimulation with antigen. However, the  
18 expression of effector molecules without *ex vivo* re-stimulation was marginal or transient, and thus how  
19 and where these CD8<sup>+</sup> T cells acquire curative effector function upon PD-1 blockade remains to be  
20 elucidated. In the anti-PD-1 cancer immunotherapy, signatures of T cells such as activation, exhaustion,  
21 cytotoxicity, IFN $\gamma$  response, and proliferation in tumor tissues have been shown to correlate with the  
22 outcome of the therapy [18-21]. However, the magnitude of up-regulation of individual genes upon  
23 anti-PD-1 therapy was limited or unspecified, making the actual activation status of T cells unintelligible.  
24 Riaz et al. estimated the number of each cell type in tumor tissues based on the gene expression profile  
25 by using an elaborated deconvolution method and demonstrated a positive correlation between the  
26 numbers of CD8<sup>+</sup> T and NK cells to the outcome of anti-PD-1 therapy [21]. Huang et al. detected the  
27 proliferation of T cells in the peripheral blood upon anti-PD-1 therapy. Intriguingly, the proliferation of  
28 CD8<sup>+</sup> T cells in relation to tumor burden showed a positive correlation to the outcome of anti-PD-1  
29 therapy, although the expression levels of Perforin and Granzymes in these proliferating CD8<sup>+</sup> T cells  
30 were rather decreased upon anti-PD-1 therapy [22].

31 Single cell analyses using mass cytometry and RNA sequencing are useful to estimate the states of  
32 individual cells and elucidate the cellular mechanisms of various biological phenomena. However, the  
33 activation of CD8<sup>+</sup> T cells upon PD-1 blockade in tumor tissues or peripheral blood was not evident  
34 even with single cell analyses. The increase of CD8<sup>+</sup> T cells with the exhausted signature or the lowest  
35 *Gzmb* expression among tumor-infiltrating lymphocytes has been reported as the hallmark of anti-PD-1  
36 therapy in single cell analyses using mass cytometry, which is rather paradoxical to its curative effects  
37 [23, 24]. By using single-cell RNA sequencing, the frequency of memory/effector-like CD8<sup>+</sup> T cells in  
38 melanoma tissues was found to correlate with the outcome of anti-PD-1 therapy [25]. However, the  
39 difference likely represents the difference in tumors and microenvironments rather than the differential  
40 response to anti-PD-1 therapy among patients because the difference was not observed between  
41 samples before and after anti-PD-1 therapy [25]. Thus, the activation of CD8<sup>+</sup> T cells upon anti-PD-1  
42 blockade has not been evident in former single cell analyses contrary to the general expectations,

1 making the cellular mechanisms of tumor-eradication and irAEs by anti-PD-1 therapy remain unclear.

2 In the current study, we performed a quantitative PCR-based single-cell expression profiling and  
3 pseudotemporal analyses to explore the trajectory of autoreactive CD8<sup>+</sup> T cells that are responsible for  
4 the fulminant type I diabetes (T1D) in NOD mice upon PD-1 blockade. First, we identified the  
5 trajectory of autoreactive CD8<sup>+</sup> T cells with four distinct states. Next we found that autoreactive CD8<sup>+</sup> T  
6 cells went through 4 activation phases. Remarkably, PD-1 strongly attenuated the transition from the  
7 second- to the third-phase, where effector functions were acquired. We further demonstrated that shifts  
8 in cluster composition markedly reflected severity of T1D in mouse. Finally, we analyzed the gene  
9 expression in melanomas of human patients. Genes representing functionally enabled T cells upon  
10 PD-1-blockade in T1D showed higher expression in melanoma tissues of responders after anti-PD-1  
11 therapy. Furthermore, genes representing active suppression by PD-1 in T1D showed higher expression  
12 in melanoma tissues of responders before anti-PD-1 therapy. These results suggest that tumor-specific T  
13 cells are activated in a similar trajectory as in T1D to destroy tumors in responders upon PD-1 blockade.

## 14 **2. Materials and methods**

### 15 2.1. Mice

16 NOD/ShiJcl mice were purchased from Japan CLEA and housed under specific pathogen-free  
17 conditions in environmentally controlled clean rooms. All mouse protocols were approved by the  
18 Animal Experimentation Committee of Tokushima University.

### 19 2.2. Induction of T1D

20 Pre-diabetic female NOD mice (10 – 12 wks-old) were administrated intraperitoneally every other day  
21 with anti-PD-L1 Ab (1-111A, 500 µg)[26]. Mice were considered diabetic after two consecutive blood  
22 glucose measurements exceeded 250 mg/dL. Rat IgG2a (BioXCell) was used for control. CD4<sup>+</sup> and  
23 CD8<sup>+</sup> T cells were depleted by the intra venous injection of Abs against CD4 (GK1.5, 200 µg) and CD8  
24 (53-6.7, 200 µg) on days -3, 1, and 5.

### 25 2.3. Isolation of islet-infiltrating lymphocytes

26 Islet infiltrates were prepared from pre-diabetic NOD mice treated with or without anti-PD-L1 Ab as  
27 previously described [27]. Briefly, pancreata were dispersed into single-cell suspensions by collagenase  
28 (Wako) and DNase I (Sigma-Aldrich). Islet-infiltrating lymphocytes were enriched by Percoll gradient  
29 centrifugation (GE Healthcare).

### 30 2.4. Detection of proliferating cells in mice

31 Pre-diabetic NOD mice were treated with or without anti-PD-L1 Ab on days 0 and 2 and EdU  
32 (5-ethynyl-2'-deoxyuridine, 1mg) on day 2. Pancreatic infiltrates, pancreatic LN cells, and spleen cells  
33 were prepared on day 4. Ghost (TNBO, 13-0870) was used to distinguish live from dead cells.  
34 EdU-incorporated cells were detected using Click-iT™ Plus Alexa Fluor™ 647 Picolyl Azide Toolkit  
35 (Invitrogen™) according to the manufacturer's instructions.

### 36 2.5. Flowcytometric analysis

37 Splenocytes, islet-infiltrating lymphocytes, and pancreatic LN cells were stained with indicated

1 antibodies. Data were obtained with Gallios (Beckman Coulter) and analyzed using FlowJo (Tree Star)  
2 or CytoBank (Cytobank). Fluorochrome-conjugated Abs against mouse CD3e (145-2C11), mouse  
3 TCR $\beta$  (H57-597), mouse CD8 $\alpha$  (53-6.7), mouse CD4 (GK1.5 and RM4-5), mouse/human CD44  
4 (IM7), mouse CD45 (30-F11), mouse CD62L (MEL-14), mouse CD69 (H1.2F3), human/mouse/rat  
5 ICOS (C398.4A), mouse CD366 Tim-3 (RMT3-23), and mouse PD-1 (RMP1-30), biotinylated Abs  
6 against mouse/human CD11b (M1/70), mouse CD11c (N418), mouse CD45R/B220 (RA3-6B2),  
7 mouse Gr1 (RB6-8C5), mouse Ter-119 (TER-119), and mouse PD-1 (RMP1-30) mAb, and Brilliant  
8 Violet 421-conjugated streptavidin were purchased from Biolegend. PE-conjugated streptavidin was  
9 purchased from BD Pharmingen. Propidium Iodide was used to distinguish live from dead cells.

## 10 11 2.6. Single cell expression profiling

12 Islet-infiltrating lymphocytes were stained with biotinylated Abs against CD11b, CD11c, CD45R/B220,  
13 Gr1, and Ter-119 together with fluorochrome-conjugated Abs against CD8 $\alpha$ , CD4, and PD-1.  
14 Biotinylated Abs were detected with streptavidin-BV421. PD-1<sup>+</sup>CD8<sup>+</sup> T cells were sorted from  
15 islet-infiltrating lymphocytes using MoFlo XDP (Beckman Coulter). Single cells of sorted PD-1<sup>+</sup>CD8<sup>+</sup>  
16 T cells were captured and lysed on chip using the C<sub>1</sub> Single-Cell Auto Prep System (Fluidigm). Reverse  
17 transcription and pre-amplification of cDNA library were performed on chip according to the  
18 manufacturer's instructions using a pool of 138 primer pairs specific to genes that are known to function  
19 in immune cells. Single-cell real-time quantitative PCR analyses were performed using nested primer  
20 pairs and 2x SsoFast EvaGreen Supermix with Low ROX (BioRad) in 96.96 Dynamic Array IFCs on  
21 the BioMark HD system (Fluidigm) according to the manufacturer's instructions. Based on Ct values  
22 calculated by the Biomark software, expression levels of genes in each single cell were calculated  
23 (Supplemental dataset 1). Out of 178 cells, 3 cells with *Gapdh* expression values falling outside the 95%  
24 confidence interval were excluded from subsequent analyses. ANOVA was performed using the  
25 SINGuLAR Analysis Toolset v3.5.2 (Fluidigm). Heat maps, violin plots, and volcano plots were  
26 generated using the ggplot2 R package. PCA was performed using the ade4 R package. To cluster  
27 single cells, K-means<sup>++</sup> clustering was performed using the LICORS R package.

## 28 29 2.7. Pseudotemporal ordering

30 The Monocle2 package was used to analyse trajectories of cells in order to discover activation  
31 transitions. 'DDRTree' was applied to reduce dimensions and the visualization functions  
32 'plot\_cell\_trajectory' or 'plot\_complex\_cell\_trajectory' were used to plot the minimum spanning tree  
33 on cells.

## 34 35 2.8. Dimensionality reduction

36 Visual stochastic neighbour embedding (viSNE) analysis was performed on cytometry data using  
37 Cytobank (Cytobank).

## 38 39 2.9. Quantitative PCR

40 Total RNA was extracted from the single-cell suspension of pancreas using TRIzol (Ambion) and  
41 subjected to reverse transcription using High-Capacity cDNA Reverse Transcription Kit (Applied  
42 Biosystems). Gene expression was analyzed by quantitative PCR using Power SYBR Green PCR

1 Master mix (Applied Biosystems) on a 7900HT Fast Real-time PCR (Applied Biosystems). Values  
2 were normalized to the expression of *Gapdh*. Specific primer sets are listed in Supplemental Table 1.

### 3 4 2.10. Gene expression in human melanoma samples

5 Normalized fragments per kilobase per million mapped reads (FPKM) of genes in human melanoma  
6 samples before or after the anti-PD-1 therapy with Nivolumab were obtained from Gene Expression  
7 Omnibus dataset (GSE91061). We examined the expression levels of genes that showed higher  
8 expression in C1–2 cells compared with C3–4 cells in human melanoma samples after the anti-PD-1  
9 therapy. We also examined the expression levels of genes that showed higher expression in C3–4 cells  
10 compared with C6 cells in human melanoma samples before the anti-PD-1 therapy. Patients were  
11 divided into responders (complete response, CR or partial response, PR), stable disease (SD), and  
12 non-responders (progressive disease, PD) according to the curative effects of anti-PD-1 therapy.  
13 Expression levels of genes were compared among three groups. Box plots were generated using the  
14 ggplot2 R package.

### 15 16 2.11. Statistics.

17 Two-tailed paired Student's t-test was used to evaluate statistical significance unless otherwise indicated.  
18  $p < 0.05$  was considered statistically significant.

## 19 20 **3. Results**

### 21 **3.1. CD8<sup>+</sup> T cells are pathogenic in the fulminant T1D of NOD mice upon PD-1 blockade**

22 PD-1 persistently suppresses the activity of autoreactive T cells in pre-diabetic NOD mice as evidenced  
23 by the rapid induction of T1D upon PD-1-blockade with anti-PD-L1 Ab and the early onset of T1D in  
24 NOD-*Pdcd1*<sup>-/-</sup> mice (Fig. 1A)[28-30]. CD8<sup>+</sup> T cells play the pathogenic role in this rapid manifestation  
25 of T1D because the depletion of CD8<sup>+</sup> but not CD4<sup>+</sup> T cells strongly attenuated the development of  
26 T1D upon PD-1-blockade (Fig. 1A). About 30% of islet-infiltrating CD8<sup>+</sup> T cells in pre-diabetic NOD  
27 mice expressed PD-1, suggesting that these PD-1<sup>+</sup>CD8<sup>+</sup> T cells were under the control of PD-1. Upon  
28 PD-1-blockade with anti-PD-L1 Ab, islet-infiltrating CD8<sup>+</sup> T cells were rapidly activated to express  
29 PD-1 and start proliferation (Fig. 1B and Supplemental Fig. 1). These CD8<sup>+</sup> T cells are beyond the  
30 control of PD-1 and likely included autoreactive CD8<sup>+</sup> T cells that actively destroyed  $\beta$  cells. Although  
31 PD-1-expressing and proliferating CD8<sup>+</sup> T cells were markedly increased in islets, their increases were  
32 insignificant or marginal in pancreatic LNs and spleen, suggesting that PD-1 mainly functions in target  
33 organs rather than in draining LNs in the regulation of autoreactive CD8<sup>+</sup> T cells in NOD mice as  
34 suggested before (Supplemental Fig. 1)[30-32]. Therefore, we focused on islet-infiltrating PD-1<sup>+</sup>CD8<sup>+</sup>  
35 T cells in the subsequent analyses.

### 36 37 **3.2. Clustering of autoreactive CD8<sup>+</sup> T cells under or beyond the control of PD-1**

38 To characterize autoreactive CD8<sup>+</sup> T cells under or beyond the control of PD-1, we prepared single  
39 PD-1<sup>+</sup>CD8<sup>+</sup> T cells from pancreata of pre-diabetic NOD mice with or without PD-1-blockade  
40 (PD1posA and PD1posC cells for PD-1 positive cells of Ab-treated and control mice, respectively)(Fig.  
41 1B). Islet-infiltrating PD-1<sup>-</sup>CD8<sup>+</sup> T cells from pre-diabetic NOD mice without PD-1-blockade were  
42 used as control (PD1negC cells). We evaluated the expression of 139 genes by quantitative PCR in a

1 total of 175 single cells (PD1posA; 82 cells from 2 mice, PD1posC; 49 cells from 12 mice, and  
2 PD1negC; 44 cells from 9 mice) and clustered single cells into 6 groups (C1–6 clusters) by using  
3 k-means<sup>++</sup> based on their gene expression profiles (C1; 14 cells, C2; 24 cells, C3; 28 cells, C4; 34 cells,  
4 C5; 35 cells, and C6; 40 cells) (Fig. 1C). To explore the molecular identities of single cells, we  
5 performed global principal component analysis (PCA) projection of all single cells profiled in this  
6 analysis. PD1posA, PD1posC and PD1negC cells were largely separated with substantial overlaps by  
7 PCA (Fig. 1D). We could also observe a clear separation of C1–6 cells by PCA (Fig. 1E).  
8 Activation-signature genes such as *Cd44*, *Cd38*, and *Icos* showed negative contribution to PC1 (Fig. 1F),  
9 suggesting that C1–4 cells represent activated cells and the magnitude of activation likely increase in the  
10 order of C4 to C1. Negative contribution of naive-signature genes such as *Sell* (CD62L), *Ccr7*, and *Lef1*  
11 to PC2 suggests that C5 cells represent naive cells. On the other hand, C6 cells had high PC1 and PC2  
12 values, suggesting that these cells represent antigen-experienced but inactivated cells that may resemble  
13 exhausted T (Tex) cells in chronic viral infection [33].

14 The composition of clusters largely differed among PD1posA, PD1posC, and PD1negC cells.  
15 Naive C5 cells predominated in PD1negC cells, in agreement with the activation-dependent expression  
16 of PD-1 (Fig. 1G)[34]. The frequencies of activated C1–C4 cells were largely differed between  
17 PD1posA and PD1posC cells (95% vs. 35% for PD1posA and PD1posC cells, respectively).  
18 Remarkably, activated PD1posC cells were composed of C3 and C4 cells, whereas PD1posA cells  
19 included C1 and C2 cells in addition to C3 and C4 cells, indicating that PD-1 restrains the transition  
20 from C3 to C2. More than half of PD1posC cells were clustered in C6, suggesting that these  
21 autoreactive CD8<sup>+</sup> T cells were inactivated by PD-1 engagement (Fig. 1G).

22

### 23 **3.3. Delineation of the activation trajectory of autoreactive CD8<sup>+</sup> T cells by pseudotemporal** 24 **ordering**

25 To explore the continuum of activation states in autoreactive CD8<sup>+</sup> T cells, we performed  
26 pseudotemporal ordering of the single cells by using Monocle 2 [35]. We could reconstruct a trajectory  
27 with two branches and four distinct states (Sa to Sd). We detected 69, 23, 44, and 39 cells on the path to  
28 Sa, Sb, Sc, and Sd, respectively (Fig. 2A–D and Supplemental Fig. S2A). C5 and C6 cells were  
29 concentrated at Sd and Sc tips of the tree, respectively, indicating that these cells are substantially distant  
30 from the other cells in pseudotime (Fig. 2, A, C, and D). As for activated C1–4 cells, C1–3 cells lined up  
31 on the path to Sa in this order, while the majority of C4 cells occupied the Sb tip of the tree. PD1posA  
32 cells were mainly composed of C1, C2, and C3 cells of Sa and C4 cells of Sb (Supplemental Fig. S2B).  
33 On the other hand, the majority of PD1posC and PD1negC cells were C6 cells of Sc and C5 cells of Sd,  
34 respectively (Supplemental Fig. S2B). The activation-signature of cells (expression levels of *Cd44*,  
35 *Cd69*, *Cxcr3*, *Fasl*, *Gzma*, *Gzmb*, *Il2ra*, and *Tnf*) showed progressive increase along the trajectory from  
36 Sb to Sa, suggesting that autoreactive CD8<sup>+</sup> T cells were activated sequentially from Sb to Sa (Fig. 2E).  
37 In the trajectory from Sa to Sd, the naive-signature of cells (expression levels of *Ccr7*, *Lef1*, and *Sell*)  
38 was progressively increased toward Sd, confirming that Sd represents naive state (Fig. 2F). On the other  
39 hand, cells near Sc showed low naive- and activation-signatures, indicating that Sc represents  
40 inactivated state (Fig. 2G).

41

### 42 **3.4. PD-1 interrupts the activation trajectory of autoreactive CD8<sup>+</sup> T cells to prohibit their**

## 1 **acquisition of effector functions**

2 To further examine the activation trajectory of islet-infiltrating CD8<sup>+</sup> T cells, we examined differentially  
3 expressed genes among different clusters. As expected, naive-signature genes were highly expressed in  
4 C5 cells, confirming that C5 represents migratory naive cells (Fig. 3A). When C1–4 cells were  
5 compared individually with C5 cells, the number of up-regulated genes was additively increased in the  
6 order of C4 to C1 (14, 43, 77, and 102 genes in C4, C3, C2, and C1 vs. C5 comparisons, respectively),  
7 further supporting the sequential activation of autoreactive CD8<sup>+</sup> T cells in this order (Fig. 3, A and B,  
8 and Supplemental Figs. 3 and 4). The expression levels of *Klf2*, *Ccr7*, *Lef1*, and *Id3* were decreased in  
9 C4 compared with C5 but increased in C3 (Fig. 3C and Supplemental Fig. S5). Because these genes  
10 have been reported to show a biphasic expression pattern with transient down-regulation in the initial  
11 phase of T cell activation [36–40], C4 likely represents primed cells that have immigrated from draining  
12 lymph nodes and C3 represents re-activated cells in islets.

13 At the transition from C4 to C3, we found the up-regulation of a variety of genes including those  
14 related to activation (e.g., *Cd5* and *Cd44*), migration (e.g., *Ccl3* and *Selplg*), and proliferation (e.g.,  
15 *Cd38*, *Foxo1*, and *Cdk4*) (Fig. 3D and Supplemental Fig. S5). FoxO1 has been reported to hinder the  
16 effector differentiation of CD8<sup>+</sup> T cells by up-regulating *Pdcd1* [41, 42], suggesting that the activation  
17 of CD8<sup>+</sup> T cells was attenuated by FoxO1–PD-1 axis at C3, which is in agreement with the interruption  
18 of the C3 to C2 transition by PD-1 among PD1posC cells as mentioned above (Fig. 1G). Upon  
19 transition to C2, more diverse genes including those related to effector function (e.g., *Gzma* and *Gzmb*)  
20 and cytokine signaling (e.g., *Stat3* and *Akt1*) were up-regulated, indicating that autoreactive CD8<sup>+</sup> T  
21 cells acquire effector function at this step and PD-1 particularly prohibits the acquisition of effector  
22 function by autoreactive CD8<sup>+</sup> T cells (Fig. 3E and Supplemental Fig. S5). C1 cells likely include  
23 terminal effector and precursors of memory CD8<sup>+</sup> T cells because the expression of genes related to  
24 terminal effector and memory T cells such as *Cd27*, *Il2rb*, *Akt1*, *Id2*, and *Batf* were markedly increased  
25 at this step (Fig. 3F and Supplemental Fig. S5)[43–45].

26

## 27 **3.5. PD-1<sup>+</sup>CD8<sup>+</sup> autoreactive T cells subjected to PD-1 blockade are functionally enabled**

28 None of the genes examined was significantly up-regulated in C6 cells compared with C1–4 cells and  
29 only two genes, *Ccl5* and *Klrc1* showed significant up-regulation in C6 cells compared with C5 cells  
30 (Fig. 4A). Interestingly, the difference in *Pdcd1* expression between C6 and C5 cells was not  
31 statistically significant, although the majority of C6 cells but not C5 cells expressed PD-1 protein on  
32 their cell surface. This discrepancy is most likely due to the generation of mRNA prior to protein and  
33 the differences in the stabilities of *Pdcd1* mRNA and PD-1 protein. Nonetheless, C6 cells expressed  
34 substantial number of genes related to metabolism, proliferation, and signal transduction such as *Idh2*,  
35 *Mdh2*, and *Akt2* at comparable levels ( $-2 < FC < 2$ ) with C1–4 and C5 cells, indicating that C6 cells  
36 maintain the basal metabolic, proliferative, and signaling capacities (Fig. 4B and Supplemental Fig. S6).  
37 Against our initial expectation that C6 cells may represent Tex-like cells, they did not substantially  
38 express genes related to exhausted, anergic, and senescent T cells, suggesting that C6 cells are  
39 intensively inactivated but are different from Tex cells (Fig. 4C)[33, 46, 47].

40 The expression of multiple inhibitory receptors such as PD-1, Tim-3, LAG-3, and BTLA is widely  
41 regarded as a hallmark of T cell exhaustion [33]. In the current study, the frequency of cells expressing  
42 multiple inhibitory receptors among PD-1<sup>+</sup> cells was increased by PD-1-blockade (Fig. 4D). However,



1 cells with multiple inhibitory receptors were concentrated in C1–2 cells and preferentially expressed  
2 multiple cytokines (Fig. 4D–F), indicating that these cells had escaped from the suppression by  
3 inhibitory receptors and were activated. Hereafter, we call C1 and C2 cells as T enabled (Ten) cells,  
4 because these cells were not exhausted but functionally enabled by PD-1 blockade.

5 Although C1–2 Ten cells were highly activated by escaping PD-1 suppression, not all C1–2 Ten  
6 cells expressed effector molecules. So, we explored genes that were differentially expressed in C1–2  
7 Ten cells with or without *Gzma/Gzmb*-expression (Fig. 4G). Among inhibitory molecules, *Btla* and  
8 *Cd160* but not *Lag3*, *Ctla4*, and *Pdcd1* were highly expressed in activated C1–2 Ten cells without  
9 *Gzma/Gzmb* expression, suggesting that BTLA and CD160 may play complementary roles in the  
10 suppression of autoreactive CD8<sup>+</sup> T cells when PD-1 function is blocked. The expression of *Havcr2*  
11 (Tim-3) and *Cd244* (2B4) was rather higher in C1–2 Ten cells expressing effector molecules,  
12 suggesting that these receptors may function in the ensuing phase. Meanwhile, C1–2 Ten cells without  
13 *Gzma/Gzmb* expression likely represent memory-precursors because they highly expressed  
14 memory-related genes such as *Eomes*, *Cd27*, *Il2rb*, and *Ccr7* [44].

### 15 16 **3.6. Cluster composition of autoreactive CD8<sup>+</sup> T cells correlates with disease status of T1D in** 17 **NOD mice**

18 Then we examined the pathological consequence of the shifts in cluster composition. Because there are  
19 substantial interindividual differences in the progression of T1D in NOD mice, we examined the  
20 possible correlation between the cluster composition and the severity of insulinitis among individual  
21 pre-diabetic NOD mice. We clustered islet-infiltrating PD-1<sup>+</sup>CD8<sup>+</sup> T cells into five groups by using  
22 k-means<sup>++</sup> based on the flowcytometric data, because PD-1<sup>+</sup>CD8<sup>+</sup> T cells were mostly divided into five  
23 clusters (i.e., C1 to C4 and C6) in the aforementioned single-cell gene expression analyses (Fig. 1).  
24 When we visualized these cells by t-SNE, five groups of cells were clearly separated (Fig. 5, A and B).  
25 We designated these five groups as C1–4 and C6-like clusters based on expression profiles of molecules.  
26 The frequencies of C1- and C2-like Ten cells were higher while the frequencies of C4-, and C6-like  
27 cells were lower in mice treated with anti-PD-L1 Ab in consistent with the results of single-cell gene  
28 expression analyses (Fig. 5C). We evaluated the destruction of  $\beta$  cells and the severity of insulinitis by  
29 quantifying the expression of genes related to  $\beta$  cells and lymphocytes in the pancreatic cell suspension  
30 of the same mouse. The expression levels of *Ins1* and *Gcg* but not *Amy2a* and *Lpl* that represent  
31 exocrine cells in pancreata showed negative- and positive-correlations to the frequencies of C1/2-like  
32 Ten and C6-like cells, respectively (Fig. 5D). Thus, mice with more C1/2-like Ten cells maintained less  
33  $\beta$  cells. The expression levels of *Cd3e*, *Cd38*, *Ifng*, *Prfl*, *Gzma*, and *Gzmb* showed positive and negative  
34 correlations to the frequencies of C1/2-like Ten and C6-like cells, respectively. These results  
35 demonstrate that the activation status of CD8<sup>+</sup> T cells markedly reflects the destruction of  $\beta$  cells and the  
36 severity of insulinitis.

### 37 38 **3.7. Tumor-specific T cells are activated in a similar trajectory found in T1D to destroy** 39 **tumor-tissues in human melanoma patients upon anti-PD-1 therapy**

40 Finally, we examined the possible involvement of a similar activation trajectory in tumor-specific T  
41 cells of human patients receiving anti-PD-1 therapy (Fig. 6A). We hypothesized that tumor-specific T  
42 cells are activated in a similar trajectory found in T1D to destroy tumor-tissues. To test this hypothesis,

1 we analyzed the data deposited by Chan and colleagues (GSE91061), in which the expression of genes  
2 in tumor-tissues before and after anti-PD-1 therapy and the responses of patients were collected [21].  
3 Remarkably, genes representing the signature of C1–2 Ten cells (i.e., genes highly expressed in C1–2  
4 Ten cells compared with C3–4 cells) showed higher expression in melanoma tissues of responders  
5 compared with those of non-responders after anti-PD-1 therapy (Fig. 6, B and C). These results indicate  
6 that tumor specific T cells need to be activated upon anti-PD-1 therapy in a similar trajectory found in  
7 T1D to destroy tumor tissues efficiently.

8 We also hypothesized that the cluster composition of tumor-specific T cells before anti-PD-1  
9 therapy influence the efficacy of the therapy. We picked up genes that represent the signature of cells  
10 with active suppression by PD-1 (i.e., genes highly expressed in C3–4 compared with C6 cells) and  
11 examined their expression in tumor-tissues before anti-PD-1 therapy. Intriguingly, genes representing  
12 the relative increase of C3–4 over C6 showed higher expression in melanoma tissues of responders  
13 compared with those of non-responders before anti-PD-1 therapy (Fig. 6D–F). These results indicate  
14 that anti-PD-1 therapy is more efficacious when tumor-infiltrating cells are actively suppressed by PD-1  
15 (i.e., at C3–4) but are not functionally impaired (i.e., at C6) before the start of anti-PD-1 therapy. Thus,  
16 the cluster composition of T cells and the expression of genes representing the activation trajectory of  
17 CD8<sup>+</sup> T cells in tumor tissues can be useful prognostic-markers for anti-PD-1 therapy.

#### 18 19 **4. Discussion**

20 In the current study, we delineated the activation trajectory of autoreactive CD8<sup>+</sup> T cells in T1D by  
21 comparing autoreactive CD8<sup>+</sup> T cells under or beyond the control of PD-1. Autoreactive CD8<sup>+</sup> T cells  
22 went through four activation-phases and PD-1 strongly attenuated the transition from the second- to the  
23 third-phase, where autoreactive CD8<sup>+</sup> T cells acquired effector function. We detected the up-regulation  
24 of *Foxo1* in C3 cells where the stepwise activation was suspended by PD-1. Because FoxO1 has been  
25 reported to hinder the effector differentiation of CD8<sup>+</sup> T cells by up-regulating *Pdcd1* [41, 42], FoxO1–  
26 PD-1 axis may partly explain the interruption of the activation trajectory at C3 in the PD-1-sufficient  
27 condition. The majority of autoreactive CD8<sup>+</sup> T cells under the control of PD-1 showed an intensively  
28 inactivated signature and exhibited a distinct trajectory in pseudotemporal ordering.

29 The shifts in cluster composition markedly reflected the damage of target tissues and the severity  
30 of inflammation in T1D of NOD mice. In addition, genes that were up-regulated along with the  
31 activation trajectory in T1D showed higher expression in melanoma tissues of responders compared  
32 with those of non-responders in anti-PD-1 therapy, indicating that tumor specific T cells can destroy  
33 tumor-tissues efficiently in human melanoma patients upon anti-PD-1 therapy when they are  
34 successfully activated in a similar trajectory found in T1D. Besides, genes representing cells with the  
35 active but not intensive suppression by PD-1 showed higher expression in melanoma tissues of  
36 responders compared with those of non-responders before the start of anti-PD-1 therapy, which is in  
37 agreement with the higher abundance of partially exhausted tumor-infiltrating CD8<sup>+</sup> T cells in  
38 responders of anti-PD-1 therapy in the former study [19]. Thus, the fine clustering of tumor-specific T  
39 cells before anti-PD-1 therapy can be a useful strategy to predict the efficacy of anti-PD-1 therapy.  
40 Because of the limited response rates of anti-PD-1 therapy, markers to distinguish responders from  
41 non-responders are extensively explored [18-21, 48, 49]. By delineating the activation trajectory of  
42 CD8<sup>+</sup> T cells upon PD-1 blockade, we could identify genes that accurately signify the activation status

1 of CD8<sup>+</sup> T cells and demonstrate their potencies as predictive markers.

2 Today, the role of PD-1 as a suppressor of T cells is widely accepted and anti-PD-1 therapy is used  
3 worldwide. However, how CD8<sup>+</sup> T cells are activated to eradicate tumor cells or damage self-tissues  
4 upon anti-PD-1 therapy remain unclear. Actually, the increase of exhausted rather than activated CD8<sup>+</sup>  
5 T cells in tumor tissues have been observed as hallmarks of PD-1-blockade at single cell level, which is  
6 rather paradoxical to its curative effect. Wei et al. reported that CD8<sup>+</sup> T cells with Tex-like features were  
7 increased by anti-PD-1 therapy in tumors of mice and human patients using mass-cytometry [23].  
8 Gubin et al. also reported the increase of cells with the lowest *Gzmb* expression upon PD-1 blockade in  
9 mice using mass-cytometry [24]. On the other hand, Sade-Feldman et al. identified  
10 memory/effector-like clusters of CD8<sup>+</sup> T cells whose frequencies were higher in melanoma tissues of  
11 responders compared with non-responders in anti-PD-1 therapy using single-cell RNA sequencing [25].  
12 However, they reported that there was no significant change between before and after anti-PD-1 therapy,  
13 indicating that the differences were likely related to features of tumors and/or microenvironments rather  
14 than PD-1 blockade itself. Although single-cell RNA sequencing is a very powerful method, the  
15 sensitivity for the detection of low-expressing genes is rather low, which may limit the fine  
16 characterization of cells. Thus, the activation of CD8<sup>+</sup> T cells upon anti-PD-1 blockade has not been  
17 evident in former single cell analyses contrary to the general expectations, making the cellular  
18 mechanisms of tumor-eradication and irAEs by anti-PD-1 therapy remain to be clarified.

19 Compared with mass-cytometry and single-cell RNA sequencing, the current method has a  
20 limitation in the number of analyzable cells but has a better sensitivity for the detection of genes with  
21 relatively low expression [50]. In pre-diabetic NOD mice, autoreactive CD8<sup>+</sup> T cells were readily  
22 activated and destroyed pancreatic  $\beta$  cells upon PD-1 blockade. Because a substantial proportion but  
23 not all of islet-infiltrating CD8<sup>+</sup> T cells proliferated upon PD-1 blockade, islet-infiltrating CD8<sup>+</sup> T cells  
24 were likely composed of cells at diverse stages of the activation and cell cycle. We took the advantage  
25 of this rapid induction of T1D and analyzed autoreactive CD8<sup>+</sup> T cells just before they completely  
26 eradicate  $\beta$  cells. Remarkably, we could detect autoreactive CD8<sup>+</sup> T cells with 4 different activation  
27 phases among no more than 175 cells, indicating that the activation of autoreactive CD8<sup>+</sup> T cells is a  
28 rapid and dynamic process. These results highlight the importance of pinpointing CD8<sup>+</sup> T cells that are  
29 being activated and quantifying functionally relevant genes for the elucidation of the actual activation  
30 status of CD8<sup>+</sup> T cells especially in anti-PD-1 therapy.

31 Our current findings revealed the activation trajectory of autoreactive CD8<sup>+</sup> T cells in the target  
32 tissue and clearly demonstrated the rapid and massive increase of activated T cells by PD-1-blockade,  
33 which parallels with disease progression. Precise and deeper understandings of PD-1 effects on the  
34 activation trajectory of T cells are expected to elucidate the pathomechanisms of spontaneous as well as  
35 anti-PD-1 related autoimmune diseases and facilitate the rational design of immunotherapies.

### 36 37 **Author contributions**

38 HO, IO, and TO designed the experiments. HO, IO, TM, DS, RM, and KS established experimental  
39 systems and performed experiments. HO, IO, and KS analyzed the data. HO, IO, and TO wrote the  
40 manuscript with all authors contributing to writing. TO supervised the project.

### 41 42 **Conflicts of interest**

1 The authors declare no competing financial interests.

2

### 3 **Acknowledgments**

4 We thank M. Ono for helpful discussion; Y. Okamoto, M. Aoki, H. Tsuduki, and R. Matsumura for  
5 technical and secretarial assistances; other members of our laboratory for helpful discussions. This work  
6 was supported in part by the Core Research for Evolutional Science and Technology Program of the  
7 Japan Science and Technology Agency (TO), Grant-in-Aid by the Japan Society for the Promotion of  
8 Science (JP18H05417, TO; JP19H01029, TO; JP15K9132, IO), and Uehara Memorial Foundation  
9 (TO).

10

### 11 **References**

- 12 [1] J. R. Brahmer, C. G. Drake, I. Wollner, J. D. Powderly, J. Picus, W. H. Sharfman *et al.* Phase I  
13 study of single-agent anti-programmed death-1 (MDX-1106) in refractory solid tumors: safety,  
14 clinical activity, pharmacodynamics, and immunologic correlates. *J Clin Oncol*,  
15 2010;28:3167-75.
- 16 [2] Y. Iwai, M. Ishida, Y. Tanaka, T. Okazaki, T. Honjo, N. Minato. Involvement of PD-L1 on  
17 tumor cells in the escape from host immune system and tumor immunotherapy by PD-L1  
18 blockade. *Proc Natl Acad Sci U S A*, 2002;99:12293-7.
- 19 [3] T. Okazaki, S. Chikuma, Y. Iwai, S. Fagarasan, T. Honjo. A rheostat for immune responses: the  
20 unique properties of PD-1 and their advantages for clinical application. *Nat Immunol*,  
21 2013;14:1212-8.
- 22 [4] A. Ribas, J. D. Wolchok. Cancer immunotherapy using checkpoint blockade. *Science*,  
23 2018;359:1350-5.
- 24 [5] F. A. Schildberg, S. R. Klein, G. J. Freeman, A. H. Sharpe. Coinhibitory Pathways in the  
25 B7-CD28 Ligand-Receptor Family. *Immunity*, 2016;44:955-72.
- 26 [6] C. Sun, R. Mezzadra, T. N. Schumacher. Regulation and Function of the PD-L1 Checkpoint.  
27 *Immunity*, 2018;48:434-52.
- 28 [7] J. M. Chemnitz, R. V. Parry, K. E. Nichols, C. H. June, J. L. Riley. SHP-1 and SHP-2 associate  
29 with immunoreceptor tyrosine-based switch motif of programmed death 1 upon primary  
30 human T cell stimulation, but only receptor ligation prevents T cell activation. *J Immunol*,  
31 2004;173:945-54.
- 32 [8] E. Hui, J. Cheung, J. Zhu, X. Su, M. J. Taylor, H. A. Wallweber *et al.* T cell costimulatory  
33 receptor CD28 is a primary target for PD-1-mediated inhibition. *Science*, 2017;355:1428-33.
- 34 [9] H. Nishimura, T. Okazaki, Y. Tanaka, K. Nakatani, M. Hara, A. Matsumori *et al.* Autoimmune  
35 dilated cardiomyopathy in PD-1 receptor-deficient mice. *Science*, 2001;291:319-22.
- 36 [10] T. Yokosuka, M. Takamatsu, W. Kobayashi-Imanishi, A. Hashimoto-Tane, M. Azuma, T.  
37 Saito. Programmed cell death 1 forms negative costimulatory microclusters that directly inhibit  
38 T cell receptor signaling by recruiting phosphatase SHP2. *J Exp Med*, 2012;209:1201-17.
- 39 [11] R. Mizuno, D. Sugiura, K. Shimizu, T. Maruhashi, M. Watada, I. M. Okazaki *et al.* PD-1  
40 Primarily Targets TCR Signal in the Inhibition of Functional T Cell Activation. *Front Immunol*,  
41 2019;10:630.
- 42 [12] S. Chikuma, S. Terawaki, T. Hayashi, R. Nabeshima, T. Yoshida, S. Shibayama *et al.*

- 1 PD-1-mediated suppression of IL-2 production induces CD8+ T cell anergy in vivo. *J Immunol*,  
2 2009;182:6682-9.
- 3 [13] L. M. Francisco, V. H. Salinas, K. E. Brown, V. K. Vanguri, G. J. Freeman, V. K. Kuchroo *et al.* PD-L1 regulates the development, maintenance, and function of induced regulatory T cells.  
4 *J Exp Med*, 2009;206:3015-29.
- 5 [14] D. L. Barber, E. J. Wherry, D. Masopust, B. Zhu, J. P. Allison, A. H. Sharpe *et al.* Restoring  
6 function in exhausted CD8 T cells during chronic viral infection. *Nature*, 2006;439:682-7.
- 7 [15] S. D. Blackburn, H. Shin, W. N. Haining, T. Zou, C. J. Workman, A. Polley *et al.* Coregulation  
8 of CD8+ T cell exhaustion by multiple inhibitory receptors during chronic viral infection. *Nat*  
9 *Immunol*, 2009;10:29-37.
- 10 [16] C. L. Day, D. E. Kaufmann, P. Kiepiela, J. A. Brown, E. S. Moodley, S. Reddy *et al.* PD-1  
11 expression on HIV-specific T cells is associated with T-cell exhaustion and disease progression.  
12 *Nature*, 2006;443:350-4.
- 13 [17] K. E. Pauken, M. A. Sammons, P. M. Odorizzi, S. Manne, J. Godec, O. Khan *et al.* Epigenetic  
14 stability of exhausted T cells limits durability of reinvigoration by PD-1 blockade. *Science*,  
15 2016;354:1160-5.
- 16 [18] M. Ayers, J. Lunceford, M. Nebozhyn, E. Murphy, A. Loboda, D. R. Kaufman *et al.*  
17 IFN-gamma-related mRNA profile predicts clinical response to PD-1 blockade. *J Clin Invest*,  
18 2017;127:2930-40.
- 19 [19] A. I. Daud, K. Loo, M. L. Pauli, R. Sanchez-Rodriguez, P. M. Sandoval, K. Taravati *et al.*  
20 Tumor immune profiling predicts response to anti-PD-1 therapy in human melanoma. *J Clin*  
21 *Invest*, 2016;126:3447-52.
- 22 [20] A. Prat, A. Navarro, L. Pare, N. Reguart, P. Galvan, T. Pascual *et al.* Immune-Related Gene  
23 Expression Profiling After PD-1 Blockade in Non-Small Cell Lung Carcinoma, Head and  
24 Neck Squamous Cell Carcinoma, and Melanoma. *Cancer Res*, 2017;77:3540-50.
- 25 [21] N. Riaz, J. J. Havel, V. Makarov, A. Desrichard, W. J. Urba, J. S. Sims *et al.* Tumor and  
26 Microenvironment Evolution during Immunotherapy with Nivolumab. *Cell*, 2017;171:934-49  
27 e16.
- 28 [22] A. C. Huang, M. A. Postow, R. J. Orlowski, R. Mick, B. Bengsch, S. Manne *et al.* T-cell  
29 invigoration to tumour burden ratio associated with anti-PD-1 response. *Nature*, 2017;545:60-5.
- 30 [23] S. C. Wei, J. H. Levine, A. P. Cogdill, Y. Zhao, N. A. S. Anang, M. C. Andrews *et al.* Distinct  
31 Cellular Mechanisms Underlie Anti-CTLA-4 and Anti-PD-1 Checkpoint Blockade. *Cell*,  
32 2017;170:1120-33 e17.
- 33 [24] M. M. Gubin, E. Esaulova, J. P. Ward, O. N. Malkova, D. Runci, P. Wong *et al.*  
34 High-Dimensional Analysis Delineates Myeloid and Lymphoid Compartment Remodeling  
35 during Successful Immune-Checkpoint Cancer Therapy. *Cell*, 2018;175:1014-30 e19.
- 36 [25] M. Sade-Feldman, K. Yizhak, S. L. Bjorgaard, J. P. Ray, C. G. de Boer, R. W. Jenkins *et al.*  
37 Defining T Cell States Associated with Response to Checkpoint Immunotherapy in Melanoma.  
38 *Cell*, 2018;175:998-1013 e20.
- 39 [26] M. Ishida, Y. Iwai, Y. Tanaka, T. Okazaki, G. J. Freeman, N. Minato *et al.* Differential  
40 expression of PD-L1 and PD-L2, ligands for an inhibitory receptor PD-1, in the cells of  
41 lymphohematopoietic tissues. *Immunol Lett*, 2002;84:57-62.
- 42

- 1 [27] T. Maruhashi, I. M. Okazaki, D. Sugiura, S. Takahashi, T. K. Maeda, K. Shimizu *et al.* LAG-3  
2 inhibits the activation of CD4(+) T cells that recognize stable pMHCII through its  
3 conformation-dependent recognition of pMHCII. *Nat Immunol*, 2018;19:1415-26.
- 4 [28] M. J. Ansari, A. D. Salama, T. Chitnis, R. N. Smith, H. Yagita, H. Akiba *et al.* The  
5 programmed death-1 (PD-1) pathway regulates autoimmune diabetes in nonobese diabetic  
6 (NOD) mice. *J Exp Med*, 2003;198:63-9.
- 7 [29] K. C. Herold, D. A. Vignali, A. Cooke, J. A. Bluestone. Type 1 diabetes: translating  
8 mechanistic observations into effective clinical outcomes. *Nat Rev Immunol*, 2013;13:243-56.
- 9 [30] J. Wang, T. Yoshida, F. Nakaki, H. Hiai, T. Okazaki, T. Honjo. Establishment of  
10 NOD-Pdcd1<sup>-/-</sup> mice as an efficient animal model of type I diabetes. *Proc Natl Acad Sci U S A*,  
11 2005;102:11823-8.
- 12 [31] M. E. Keir, S. C. Liang, I. Guleria, Y. E. Latchman, A. Qipo, L. A. Albacker *et al.* Tissue  
13 expression of PD-L1 mediates peripheral T cell tolerance. *J Exp Med*, 2006;203:883-95.
- 14 [32] D. Sugiura, T. Maruhashi, I. M. Okazaki, K. Shimizu, T. K. Maeda, T. Takemoto *et al.*  
15 Restriction of PD-1 function by cis-PD-L1/CD80 interactions is required for optimal T cell  
16 responses. *Science*, 2019.
- 17 [33] E. J. Wherry, M. Kurachi. Molecular and cellular insights into T cell exhaustion. *Nat Rev*  
18 *Immunol*, 2015;15:486-99.
- 19 [34] Y. Agata, A. Kawasaki, H. Nishimura, Y. Ishida, T. Tsubata, H. Yagita *et al.* Expression of the  
20 PD-1 antigen on the surface of stimulated mouse T and B lymphocytes. *Int Immunol*,  
21 1996;8:765-72.
- 22 [35] X. Qiu, Q. Mao, Y. Tang, L. Wang, R. Chawla, H. A. Pliner *et al.* Reversed graph embedding  
23 resolves complex single-cell trajectories. *Nat Methods*, 2017;14:979-82.
- 24 [36] B. T. Endrizzi, S. C. Jameson. Differential role for IL-7 in inducing lung Kruppel-like factor  
25 (Kruppel-like factor 2) expression by naive versus activated T cells. *Int Immunol*,  
26 2003;15:1341-8.
- 27 [37] C. T. Kuo, M. L. Veselits, J. M. Leiden. LKLF: A transcriptional regulator of single-positive T  
28 cell quiescence and survival. *Science*, 1997;277:1986-90.
- 29 [38] A. J. Menner, K. S. Rauch, P. Aichele, H. Pircher, C. Schachtrup, K. Schachtrup. Id3 Controls  
30 Cell Death of 2B4<sup>+</sup> Virus-Specific CD8<sup>+</sup> T Cells in Chronic Viral Infection. *J Immunol*,  
31 2015;195:2103-14.
- 32 [39] T. Willinger, T. Freeman, M. Herbert, H. Hasegawa, A. J. McMichael, M. F. Callan. Human  
33 naive CD8 T cells down-regulate expression of the WNT pathway transcription factors  
34 lymphoid enhancer binding factor 1 and transcription factor 7 (T cell factor-1) following  
35 antigen encounter in vitro and in vivo. *J Immunol*, 2006;176:1439-46.
- 36 [40] C. Y. Yang, J. A. Best, J. Knell, E. Yang, A. D. Sheridan, A. K. Jesionek *et al.* The  
37 transcriptional regulators Id2 and Id3 control the formation of distinct memory CD8<sup>+</sup> T cell  
38 subsets. *Nat Immunol*, 2011;12:1221-9.
- 39 [41] R. Hess Michelini, A. L. Doedens, A. W. Goldrath, S. M. Hedrick. Differentiation of CD8  
40 memory T cells depends on Foxo1. *J Exp Med*, 2013;210:1189-200.
- 41 [42] M. M. Staron, S. M. Gray, H. D. Marshall, I. A. Parish, J. H. Chen, C. J. Perry *et al.* The  
42 transcription factor FoxO1 sustains expression of the inhibitory receptor PD-1 and survival of

- 1 antiviral CD8(+) T cells during chronic infection. *Immunity*, 2014;41:802-14.
- 2 [43] M. D. Buck, D. O'Sullivan, E. L. Pearce. T cell metabolism drives immunity. *J Exp Med*,  
3 2015;212:1345-60.
- 4 [44] S. M. Kaech, W. Cui. Transcriptional control of effector and memory CD8+ T cell  
5 differentiation. *Nat Rev Immunol*, 2012;12:749-61.
- 6 [45] G. Xin, D. M. Schauder, B. Lainez, J. S. Weinstein, Z. Dai, Y. Chen *et al.* A Critical Role of  
7 IL-21-Induced BATF in Sustaining CD8-T-Cell-Mediated Chronic Viral Control. *Cell Rep*,  
8 2015;13:1118-24.
- 9 [46] J. Crespo, H. Sun, T. H. Welling, Z. Tian, W. Zou. T cell anergy, exhaustion, senescence, and  
10 stemness in the tumor microenvironment. *Curr Opin Immunol*, 2013;25:214-21.
- 11 [47] E. J. Wherry, S. J. Ha, S. M. Kaech, W. N. Haining, S. Sarkar, V. Kalia *et al.* Molecular  
12 signature of CD8+ T cell exhaustion during chronic viral infection. *Immunity*, 2007;27:670-84.
- 13 [48] N. A. Rizvi, M. D. Hellmann, A. Snyder, P. Kvistborg, V. Makarov, J. J. Havel *et al.* Cancer  
14 immunology. Mutational landscape determines sensitivity to PD-1 blockade in non-small cell  
15 lung cancer. *Science*, 2015;348:124-8.
- 16 [49] P. C. Tumeh, C. L. Harview, J. H. Yearley, I. P. Shintaku, E. J. Taylor, L. Robert *et al.* PD-1  
17 blockade induces responses by inhibiting adaptive immune resistance. *Nature*,  
18 2014;515:568-71.
- 19 [50] T. Kroneis, E. Jonasson, D. Andersson, S. Dolatabadi, A. Stahlberg. Global preamplification  
20 simplifies targeted mRNA quantification. *Sci Rep*, 2017;7:45219.
- 21

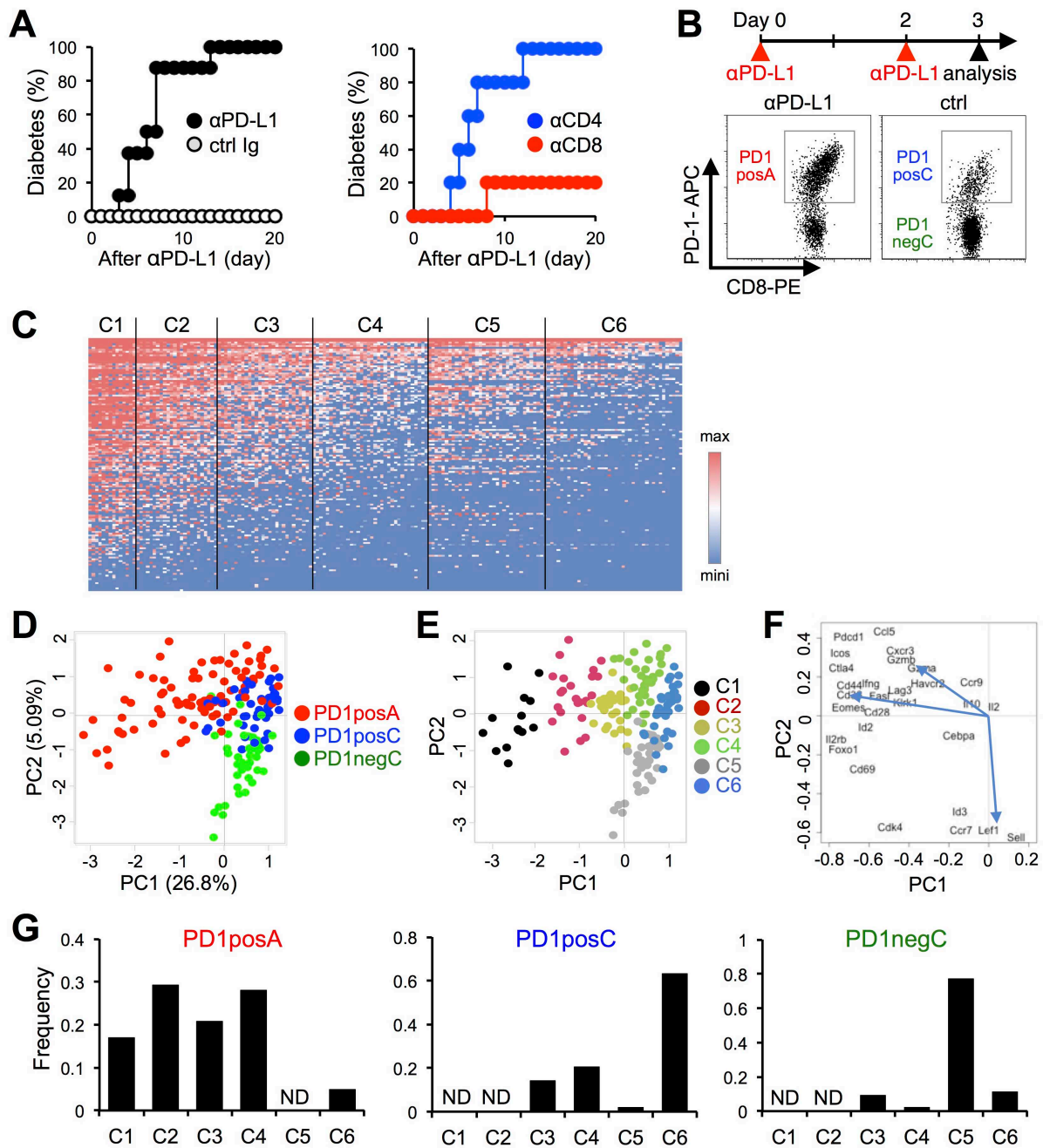
1 **Supplemental Table 1**

2	Gene	Forward primer (5' to 3')	Reverse primer (5' to 3')
3	<i>Gzmb</i>	ACAGAAGGATCGGGAGTGTG	CTATGCCTGCAGCCACTTTT
4	<i>Gzma</i>	GGCCATCTCTTGCTACTCTCC	GAACAACCGTGTCTCCTCCAA
5	<i>Prf</i>	TAGCCAATTTTGCAGCTGAG	GGTTTTTGTACCAGGCGAAA
6	<i>Ifng</i>	CCACGGCACAGTCATTGAAA	GCCAGTTCCTCCAGATATCCAA
7	<i>Cd3e</i>	CTGCTACACACCAGCCTCAA	ATCAGCAAGCCCAGAGTGAT
8	<i>Cd38</i>	CGCTGCCTCATCTACTCA	GCAAGGGTTCTTGAAACAA
9	<i>Lpl</i>	GGGAGTTTGGCTCCAGAGTTT	TGTGICTTCAGGGGTCCCTAG
10	<i>Amy2a2, 3, 4, 5</i>	TAAAGTGGCTGACAAAGCCC	AGCCTTTTCAAACCTGGTGG
11	<i>Gcg</i>	TGGTGCTCATCTCGTCAGAG	TGAATTTGAGAGGCATGCTG
12	<i>Ins1</i>	CCTGTTGGTGCACTTCCTA	TCTGAAGGTCCCCGGGGCT

13

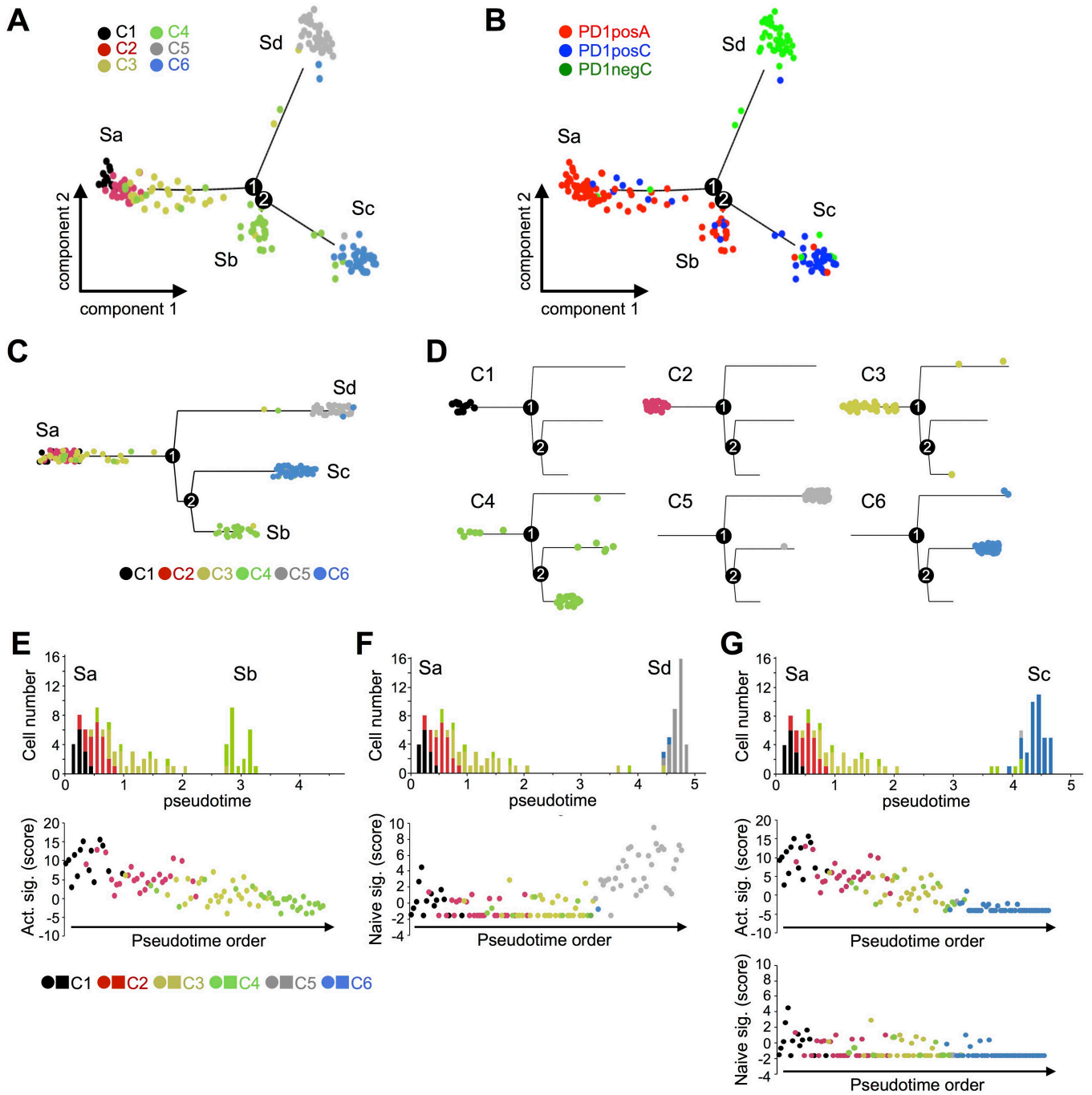
14 **Supplemental Table 1. Primer sets for real-time quantitative PCR in Fig. 5.**



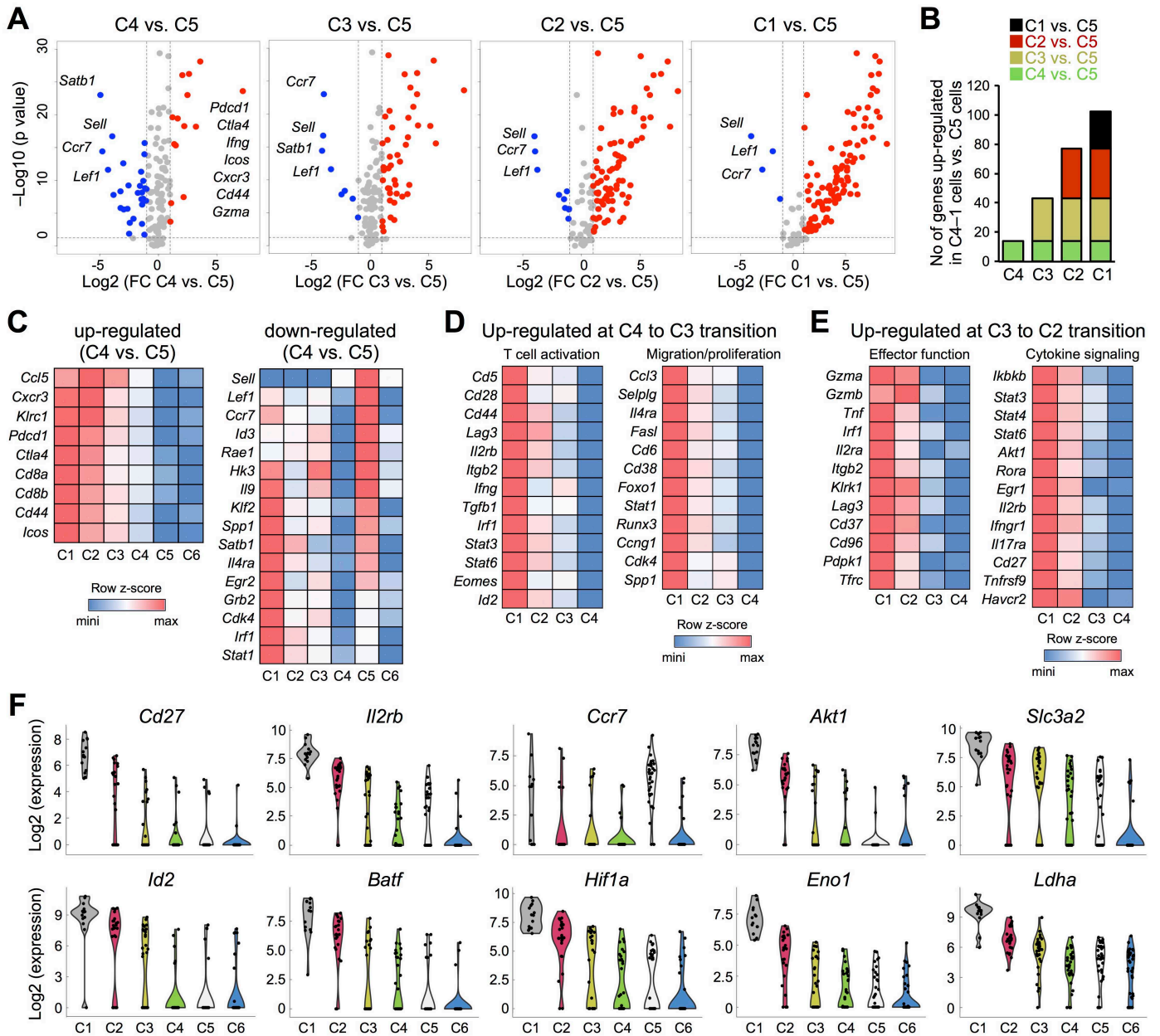
**Fig. 1**

**Fig. 1.** Clustering of autoreactive CD8<sup>+</sup> T cells under and beyond the control of PD-1. (A) Pathogenic role of CD8<sup>+</sup> T cells in the rapid manifestation of T1D in pre-diabetic NOD mice upon PD-1-blockade. Diabetic incidence of NOD mice treated with  $\alpha$ PD-L1 or its isotype control (ctrl Ig) (n = 8 each)(left). Diabetic incidence of NOD mice depleted of CD4<sup>+</sup> ( $\alpha$ CD4) or CD8<sup>+</sup> ( $\alpha$ CD8) T cells upon  $\alpha$ PD-L1 treatment (n = 5 each)(right). (B) Preparation of PD-1<sup>+</sup>CD8<sup>+</sup> T cells under or beyond PD-1 control. Schematic representation of the sample preparation (top). PD-1<sup>+</sup>CD8<sup>+</sup> T cells from  $\alpha$ PD-L1-treated NOD mice (PD1posA) and PD-1<sup>+</sup>CD8<sup>+</sup> and PD-1<sup>-</sup>CD8<sup>+</sup> T cells from control NOD mice (PD1posC and PD1negC, respectively) were analyzed (bottom). (C) Heat map showing k-means<sup>++</sup> clustering of PD1posA, PD1posC, and PD1negC cells. A total of 175 single cells were clustered based on the expression of 139 genes. (D–F) PCA of single cells. Source (D) and cluster (E) of each cell are shown by color as indicated. Correlations of genes with the principal component 1 (PC1) and PC2 from the PCA are shown (F). (G) Cluster compositions of PD1posA, PD1posC, and PD1negC cells. ND, not detected.

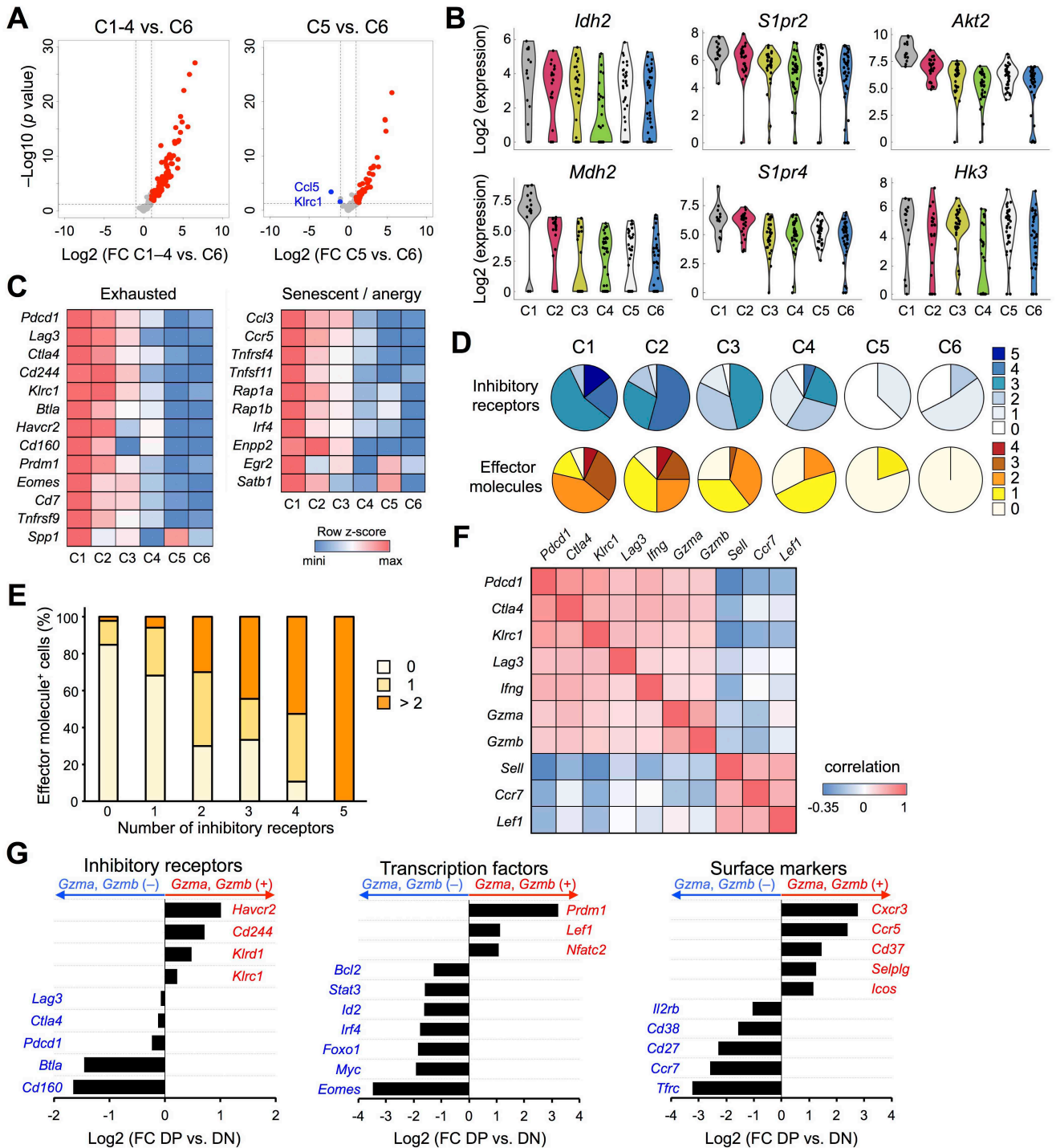
**Fig. 2**



**Fig. 2.** Activation trajectories of autoreactive CD8<sup>+</sup> T cells revealed by the pseudotemporal ordering. (A–D) Pseudotemporal ordering of single cells. Projection into a two-dimensional space (A and B) and tree structure (C and D) by Monocle 2. Four states (Sa to Sd) and two branches (1 and 2) are indicated. Cluster (A) and origin (B) of cells are colored as indicated. Tree structures of C1–6 cells are separately shown (D). (E–G) Changes in naive and activated signatures of cells along with the reconstructed trajectory. Number of cells (top) and naive and activated (Act.) signatures (sig.) of each cell (middle and bottom) plotted with respect to pseudotime and pseudotime-order, respectively. Trajectories from Sa to Sb (E), Sa to Sd (F), and Sa to Sc (G) are shown. Cluster of cells are shown by color as indicated.

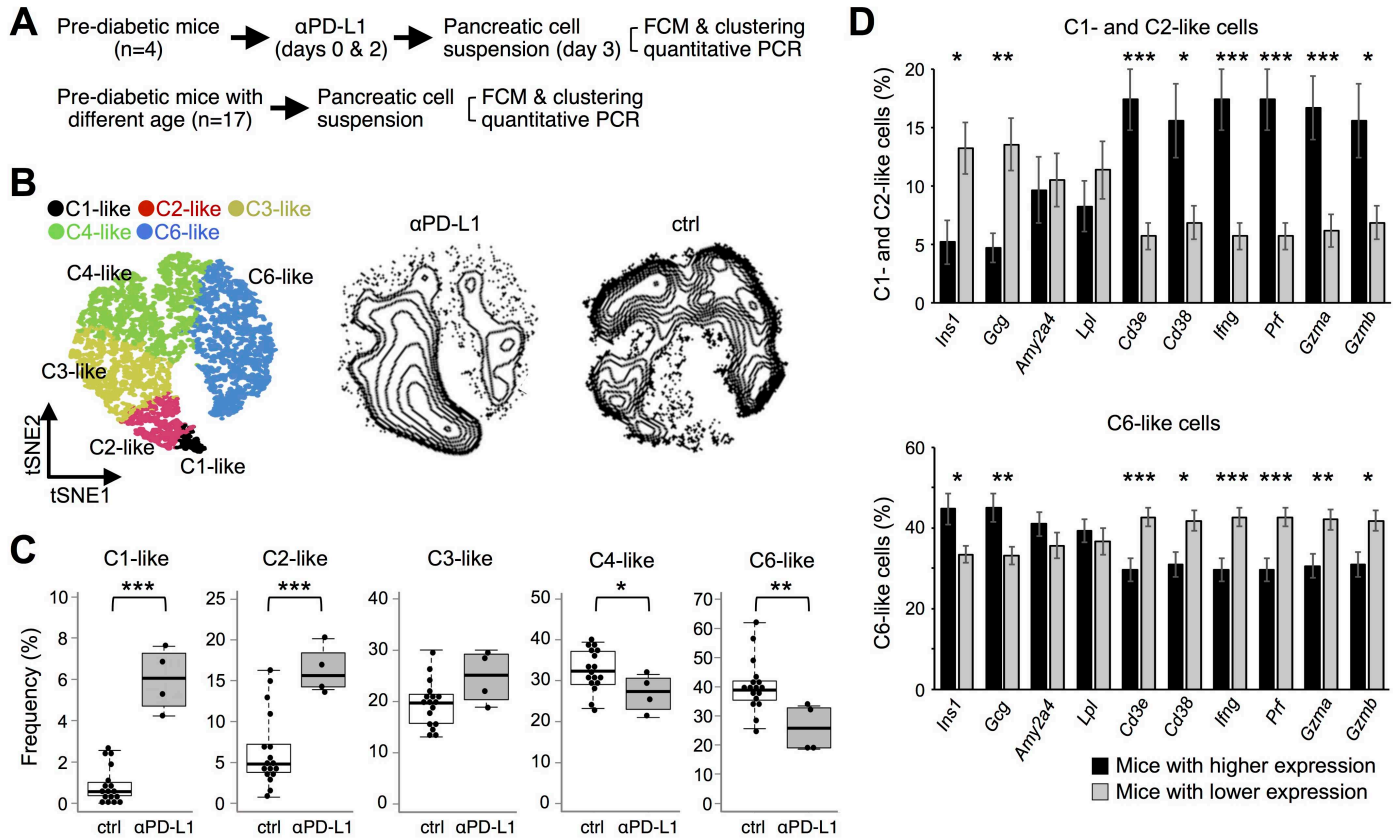
**Fig. 3**

**Fig. 3.** PD-1 prohibited autoreactive CD8<sup>+</sup> T cells from acquiring effector function. (A and B) Sequential up-regulation of genes related to T cell activation in the order of C4 to C1. Volcano plots showing differentially expressed genes between C5 and C4-1 cells (A). Stacked bar graphs indicating the number of genes that were up-regulated in C4-1 cells compared with C5 cells. Genes up-regulated more than 2 folds ( $p < 0.05$ , ANOVA test) were counted. The number of genes that was additively up-regulated at the indicated comparison is shown with the indicated color (B). (C-E) Heat maps showing the relative expression levels of indicated genes among indicated clusters. Levels of down expression (blue) or up expression (red) are shown on a normalized z-score of each gene among C1-6 (C) and C1-4 cells (D and E). Up-regulated and down-regulated genes in the comparison between C4 and C5 are shown (C). Genes up-regulated in the transition from C4 to C3 (D) and C3 to C2 (E) are shown. (F) Violin plots showing the expression of genes that were highly up-regulated in the transition from C2 to C1.

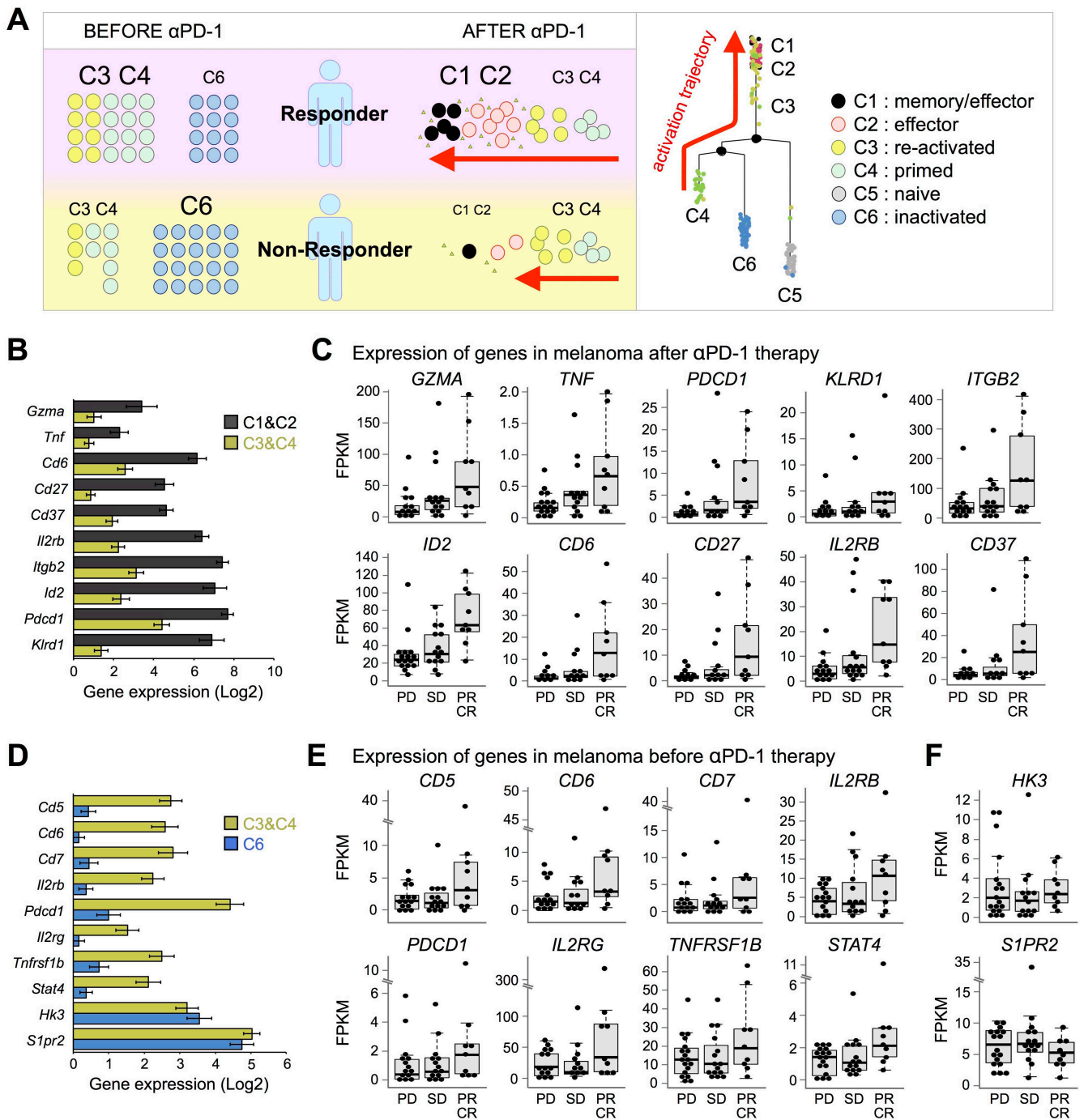
**Fig. 4**

**Fig. 4.** Preferential expression of effector molecules by cells with multiple inhibitory receptors upon PD-1 blockade. (A) Volcano plots showing differentially expressed genes between C6 and C1–4 or C5 cells. (B) Substantial expression of genes related to metabolism, proliferation, and signal transduction by C6 cells. Violin plots showing the expression of indicated genes in C1–6 cells. (C) No up-regulation of genes related to exhaustion, senescent, and anergy in C6 cells. Heat maps showing the relative expression levels of indicated genes. Levels of down expression (blue) or up expression (red) are shown on a normalized z-score of each gene. (D–F) The expression of multiple inhibitory receptors (*Pdcd1*, *Havcr2*, *Lag3*, *Btla*, and *Klrc1*) and effector molecules (*Gzma*, *Gzmb*, *Ifng*, and *Tnf*) by highly activated T cells upon PD-1 blockade. The frequencies of cells expressing indicated numbers of inhibitory receptors and effector molecules are shown for each cluster (D). The frequencies of cells expressing indicated numbers of effector molecules are shown for cells expressing indicated numbers of inhibitory receptors (E). The correlation coefficients of co-expression were evaluated by nearest-neighbor analysis for indicated gene sets (F). (G) Differentially expressed genes between C1–2 cells with or without effector molecules. Fold-change expression of indicated genes between C1–2 cells double-positive (DP, red) or -negative (DN, blue) for *Gzma* and *Gzmb* are shown in  $\text{log}_2$  scale. Genes showed higher expression in DP and DN cells are colored in red and blue, respectively.

**Fig. 5**

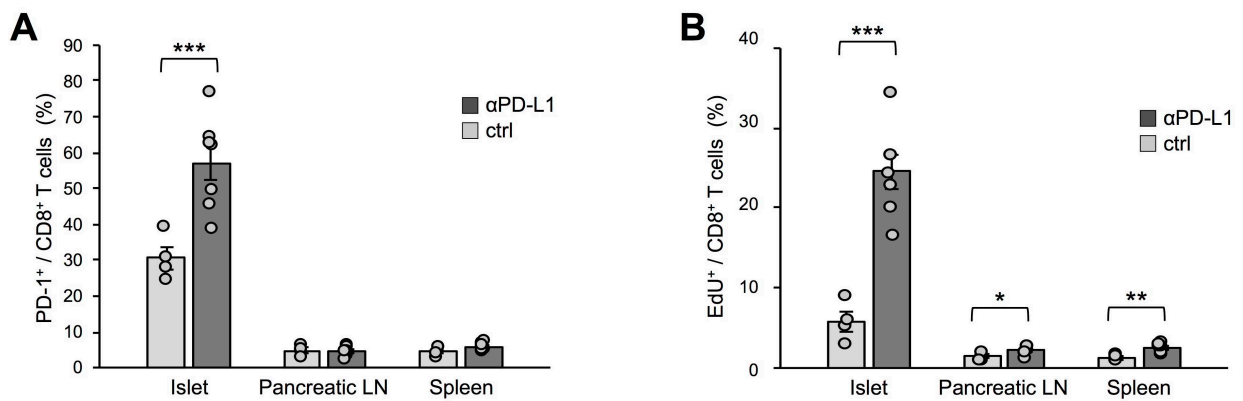


**Fig. 5.** Correlation between cluster composition and disease status of T1D in NOD mice. (A) Schematic representation of the sample preparation. Pancreatic cell suspension was divided into two for flowcytometry (FCM) and quantitative PCR. (B) Classification of PD-1<sup>+</sup>CD8<sup>+</sup> T cells into C1-, C2-, C3-, C4-, and C6-like clusters. A t-SNE plot of islet-infiltrating PD-1<sup>+</sup>CD8<sup>+</sup> T cells overlaid with the color-coded clusters (left). Density t-SNE plots of islet-infiltrating PD-1<sup>+</sup>CD8<sup>+</sup> T cells from NOD mice treated with (middle, n = 4) or without (right, n = 17)  $\alpha$ PD-L1. (C) Increase of C1- and C2-like cells and decrease of C4- and C6-like cells by PD-1 blockade. (D) Correlation between cluster composition and disease status. Frequencies of C1- and C2-like (top) and C6-like (bottom) cells are shown for mice with higher (black) and lower (gray) expression of indicated genes. Two-tailed paired Student's *t*-test (C and D). \**P* < 0.05, \*\**P* < 0.01, \*\*\**P* < 0.005.

**Fig. 6**

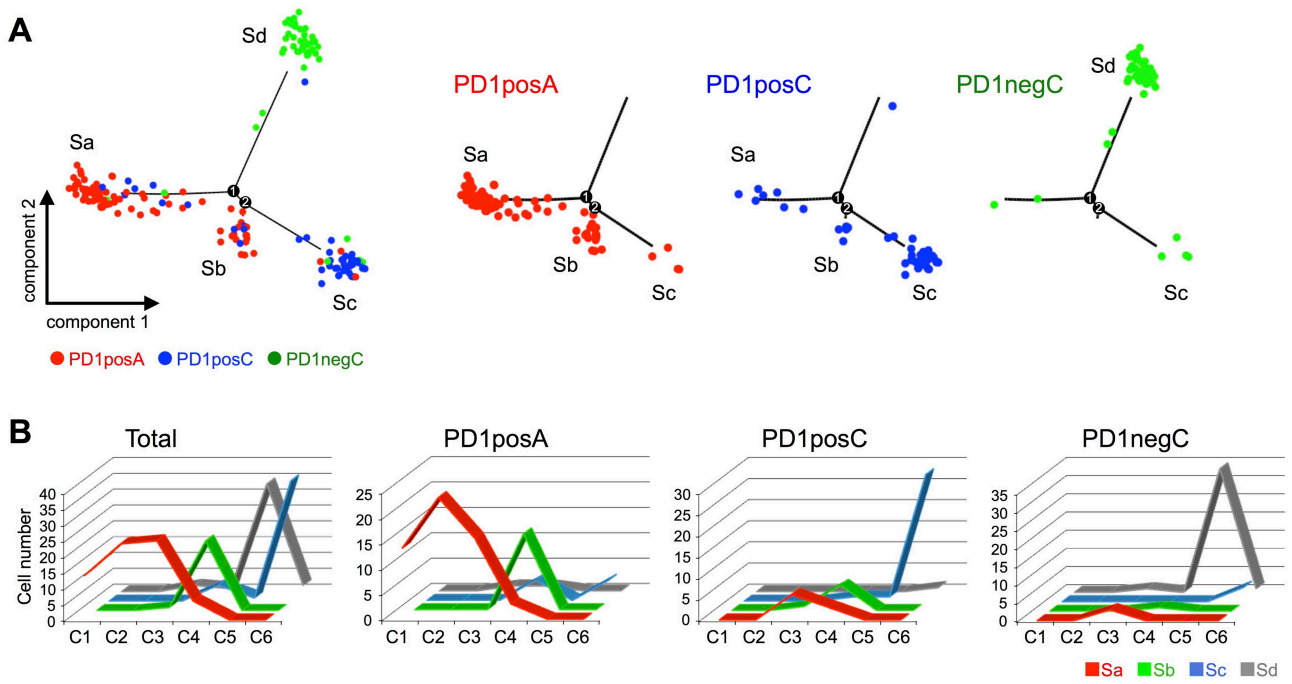
**Fig. 6.** Tumor-specific T cells are activated in a similar trajectory found in T1D to destroy tumor-tissues in human melanoma patients upon anti-PD-1 therapy. (A) Schematic representation of the two hypotheses. Anti-PD-1 therapy is expected to be more efficacious when tumor-infiltrating T cells are actively suppressed by PD-1 (i.e., at C3–4) but are not functionally impaired (i.e., at C6) before anti-PD-1 therapy (left). Anti-PD-1 therapy is expected to enable tumor specific T cells in a similar activation trajectory found in T1D in responders of anti-PD-1 therapy (middle). The activation trajectory of autoreactive CD8<sup>+</sup> T cell upon anti-PD-1 therapy in NOD mice is shown in the right side. (B and C) Genes representing the progression of the activation trajectory in T1D showed higher expression in melanoma-tissues of responders upon anti-PD-1 therapy. Bar graphs showing the expression levels of indicated genes in C1–2 and C3–4 cells (B). Box plots showing the expression levels (FPKMs) of indicated genes in melanoma-tissues upon anti-PD-1 therapy (C). (D–F) Genes representing the dominance of C3–4 over C6 in T1D showed higher expression in melanoma-tissues of responders before anti-PD-1 therapy. Bar graphs showing the expression levels of indicated genes in C3–4 and C6 cells (D). Box plots showing the expression levels of indicated genes in melanoma-tissues before anti-PD-1 therapy. Genes with higher (E) or comparable (F) expression levels in C3–4 cells compared with C6 cells are shown. PD, progressive disease (n = 18); SD, stable disease (n = 15); PR, partial response (n = 6); CR, complete response (n = 3) (C, E, and F).

## Supplemental Fig. 1



**Supplemental Fig. 1.** Activation of diabetogenic T cells in islets upon PD-1 blockade. (A) Increase of PD-1 expressing CD8<sup>+</sup> T cells in islets upon PD-1 blockade. Pre-diabetic NOD mice were treated with (n = 7) or without (n = 4)  $\alpha$ PD-L1 on days 0 and 2. PD-1 expression on CD8<sup>+</sup> T cells in islets, pancreatic LNs, and spleens were examined on day 4. (B) Increase of proliferating CD8<sup>+</sup> T cells in islets upon PD-1 blockade. Pre-diabetic NOD mice were treated with (n = 7) or without (n = 5)  $\alpha$ PD-L1 on days 0 and 2 and EdU on day 2. EdU-incorporation of CD8<sup>+</sup> T cells in islets, pancreatic LNs, and spleens were examined on day 4. Two-tailed paired Student's *t*-test. \**P* < 0.05, \*\**P* < 0.01, \*\*\**P* < 0.005.

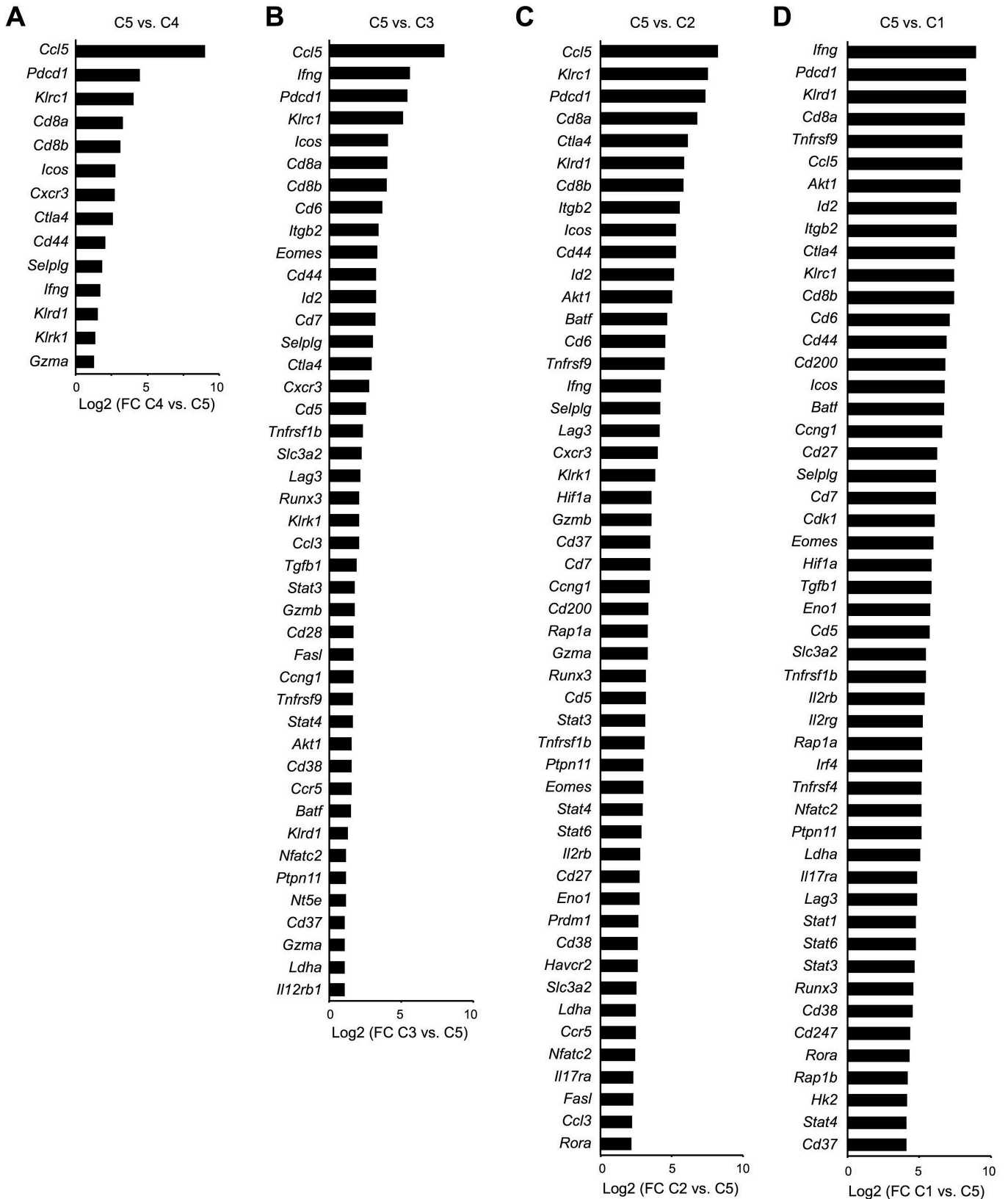
## Supplemental Fig. 2.



**Supplemental Fig. 2.** Activation trajectories of PD1posA, PD1posC, and PD1negC cells. (A) Pseudotemporal ordering of PD1posA, PD1posC, and PD1negC cells projected into a two-dimensional space. Four states (Sa to Sd) and two branches (1 and 2) are indicated. (B) The correlations between C1–C6 and Sa–Sd among total, PD1posA, PD1posC, and PD1negC single cells.

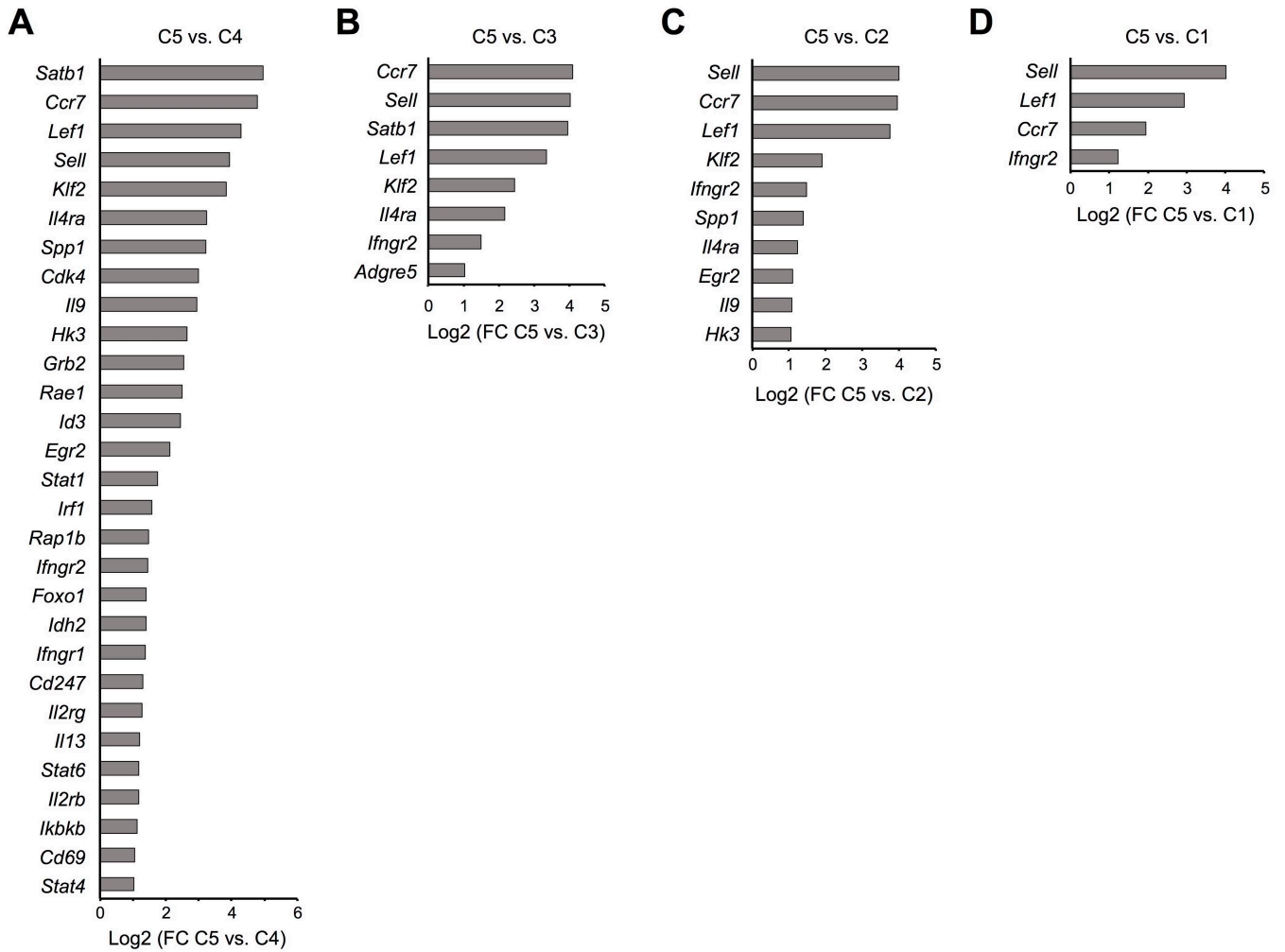


**Supplemental Fig. 3.**



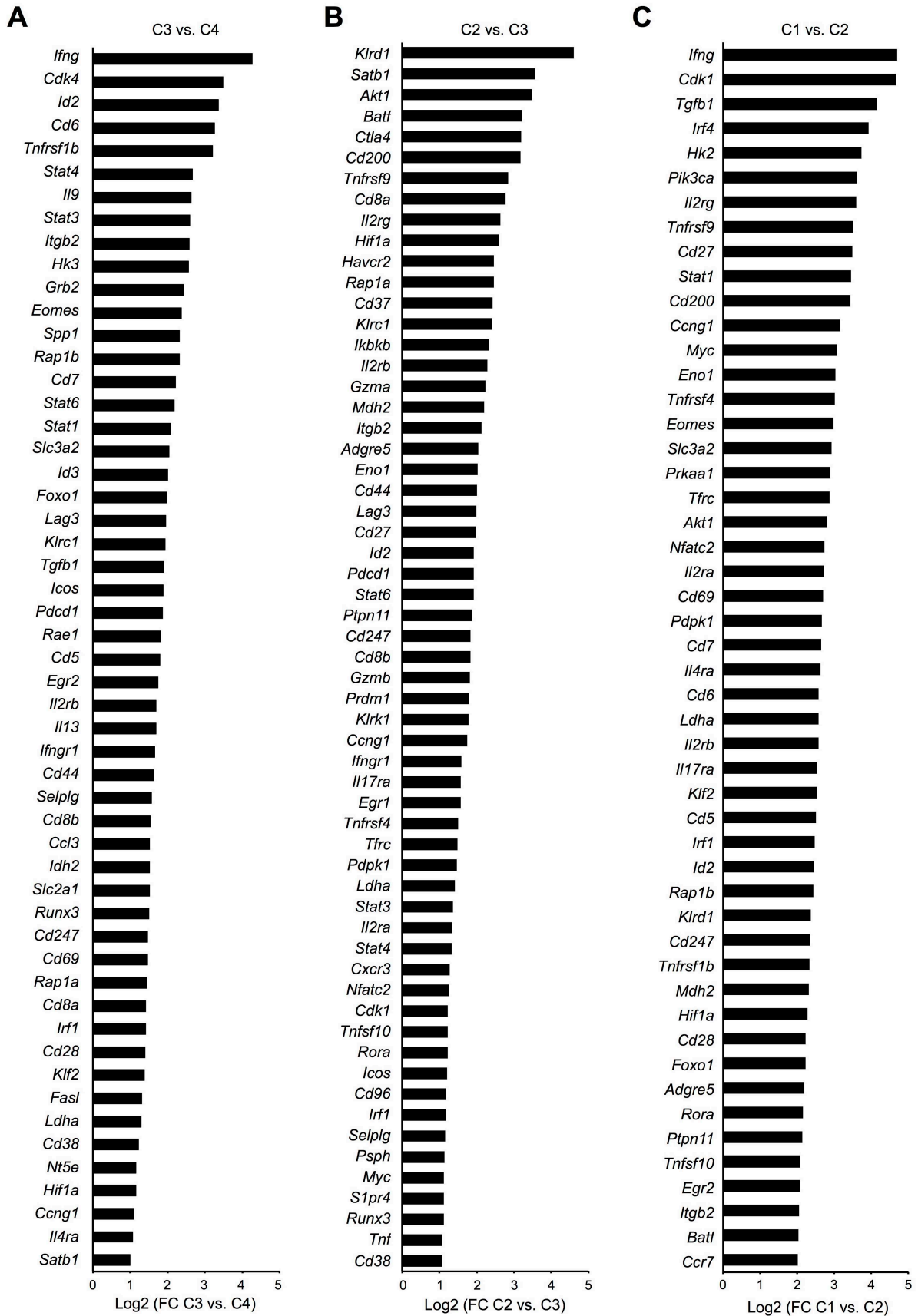
**Supplemental Fig. 3.** Up-regulated genes in C4–1 cells compared with C5 cells. (A) Genes that were up-regulated more than 2 folds in C4 cells compared with C5 cells. (B) Genes that were up-regulated more than 2 folds in C3 cells compared with C5 cells. (C) Genes that were up-regulated more than 2 folds in C2 cells compared with C5 cells. (D) Top 50 genes that were up-regulated in C1 cells compared with C5 cells. FC expression of indicated genes between cells with indicated clusters are shown in a log<sub>2</sub> scale.

**Supplemental Fig. 4.**



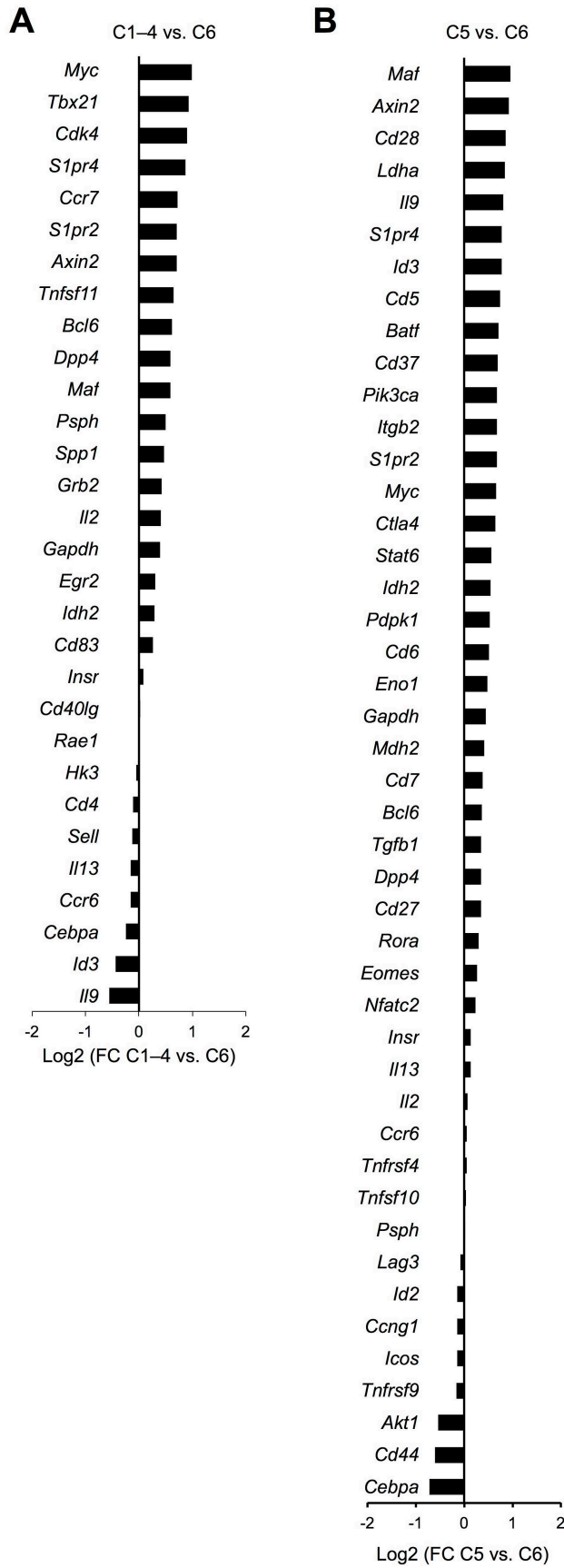
**Supplemental Fig. 4.** Down-regulated genes in C4–1 cells compared with C5 cells. (A) Genes that were down-regulated more than 2 folds in C4 cells compared with C5 cells. (B) Genes that were down-regulated more than 2 folds in C3 cells compared with C5 cells. (C) Genes that were down-regulated more than 2 folds in C2 cells compared with C5 cells. (D) Genes that were down-regulated more than 2 folds in C1 cells compared with C5 cells. FC expression of indicated genes between cells with indicated clusters are shown in a log<sub>2</sub> scale.

**Supplemental Fig. 5.**



**Supplemental Fig. 5.** Up-regulated genes at the transition from C4 to C1. (A) Genes that were up-regulated more than 2 folds in C3 cells compared with C4 cells. (B) Genes that were up-regulated more than 2 folds in C2 cells compared with C3 cells. (C) Top 50 genes that were up-regulated in C1 cells compared with C2 cells. FC expression of indicated genes between cells with indicated clusters are shown in a log<sub>2</sub> scale.

**Supplemental Fig. 6.**



**Supplemental Fig. 6.** Genes expressed comparably in C6 cells compared with C1-4 and C5 cells. (A) Genes that were expressed comparably ( $|FC| < 2$ ) in C6 cells compared with C1-4 cells. (B) Genes that were expressed comparably ( $|FC| < 2$ ) in C6 cells compared with C5 cells. FC expression of indicated genes among C6 cells compared with C1-4 (A) and C5 (B) cells are shown in a log<sub>2</sub> scale.